over time, a result implicating melanopsin in the potentiation of outer retinal signalling as this behaviour progresses. We also found that older MO mice lose the positive correlation in BLA across time due to an enhanced light aversion in the first five minutes, an intriguing finding that suggests increased potency of melanopsin signalling with advancing age in retinal degeneration.

Although we have not examined BLA in neonatal animals here, the age (8–14 days old) at which rats were used in the initial studies by Crozier and Pincus [1] strongly implicates the involvement of the melanopsin system. This is because outer retinal function does not contribute to retinal activation prior to postnatal day 10 in mice [59] and between postnatal days 12–14 in rats [60].

An important component of our behavioural paradigm is the direct comparison between behaviour in light versus complete darkness. This method takes advantage of a phenomenon whereby, in the absence of light, animals will choose to spend the majority of a 30 minute period in the front half of the arena. The incorporation of this behaviour into our data analysis may help to explain why light aversion has not been reported previously over short durations in retinally degenerate rodents.

The light:dark choice test is regarded as an unconditioned conflict paradigm, where the innate tendency for light avoidance conflicts with the propensity of mice to explore/escape novel places into which they are forced [6,7]. To the best of our knowledge the robust behaviour in darkness we report has not previously been described. Although not easy to explain, we suggest this response may relate to an anxiety state which occurs in mice forced into a novel environment [61].

When mice are given the choice to freely explore something new they display a behaviour known as "neophobia" which involves initial retreat from and then progressive exploration of the novelty. If mice are presented simultaneously with a familiar and novel compartment to freely explore, they will spend approximately 75% of their time in the novel compartment. However, when they are forced into this novel compartment the animals display heightened anxiety levels, as measured by elevated corticosterone [61]. Thus, in the context of the present experiment, under complete darkness, a state of forced novelty exists. We suggest that in the absence of the aversive stimulus of light, mice may simply be returning to the point of entry which they associate with escape to the home cage.

In adult nocturnal rodents, BLA may contribute to diurnal behaviour by moving animals away from sunlight, towards darkened nesting areas where they would sleep. In this respect, the melanopsin-dependent temporal potentiation of BLA we identify here may be of particular importance in increasing motivation to leave open field environments. Given the role for melanopsin in modulating sleep [31,32,33] it will be important to examine the interaction between BLA and this other melanopsin-modulated behaviour in future experiments.

Although not available in the present study, it would be interesting to examine the performance of melanopsin aDTA mice [12,32] in our paradigm, these mice will help to determine the extent to which the mRGC pathway is required for BLA. However, like the MKO mice reported here, mice with a targeted destruction of mRGCs retain a behavioural aversion to light [18], indicating that mRGCs are probably not an absolute requirement for BLA.

## Atropine application reveals a new element to light perception

Atropine pre-treatment led to a significant elevation of BLA in WT and MO mice, with both genotypes now responding to a similar level. The effect was particularly strong on the melanopsin component of BLA, strengthening the potentiation of this behaviour over time. In contrast, atropine failed to enhance the overall aversive response of MKO animals to light but did induce a positive correlation over time. We concluded from these experiments that BLA may normally be constrained by the PLR and that with fully dilated pupils, enhanced light stimulation of the retina increases the activity of outer and to a greater extent, inner retinal photoreceptors.

In order to control for the possibility that atropine may act independently of pupil dilation, we also added this drug to the eyes of TKO mice, which lack a PLR. To our complete surprise, this manipulation revealed an ability of TKOs to perceive light and display BLA. Previous work with these animals has shown that despite having an intact retina, they lack significant visual responsiveness [49]. Recent preliminary data indicates that TKO mice retain a small ERG with a spectral sensitivity matching rod opsin [54]. We report here that atropine application significantly enhances the b-wave component of this response and that bilateral axotomy abolishes the atropine-induced behavioural aversion to light exhibited by TKO mice. Thus, we suggest that atropine augments a residual retinal response in these animals, which is sufficient to drive BLA. In a complementary fashion, we confirm that in the absence of atropine, enhancing retinal light-responsiveness with ChR2 can also drive BLA in TKO mice in the absence of a PLR. The magnitude and temporal kinetics of this ChR2-mediated response are strikingly similar to BLA seen in WT mice, indicating that during development, the proximal neural circuitry for BLA can develop independently of normal rod, cone and melanopsin signalling. Interestingly, the behavioural effect in this experiment was achieved without significant transfection of mRGCs identified using β-galactosidase staining. Although this observation suggests that mRGCs may not be the only conduits mediating BLA, new evidence revealing an extended diversity of melanopsin expressing ganglion cells [36,62] raises the possibility that ChR2V may have been expressed in mRGCs that we could not detect.

During the preparation of this manuscript we became aware of another study examining the ability of phototransduction deficient MO mice ($Gnat1^{-/-}$, $Cnga3^{-/-}$) to perform pattern discrimination [36]. While these mice fail to respond to visual gratings in an optokinetic tracking test, in a forced-swim test, they can learn to use gratings of low spatial frequency to predict positive reinforcement (presence of an escape platform), while control TKOs ($Opn4^{-/-}$, $Gnat1^{-/-}$, $Cnga3^{-/-}$) cannot. This is accompanied by grating-induced c-Fos activation in primary visual cortex. The authors attribute these results solely to inner retinal melanopsin cells. Although no experimental data is presented, they also make the comment that control TKO mice retain an ability to discriminate between two screens in the visual learning task that vary significantly in luminance. This observation agrees with our findings of atropine-enhanced BLA and provides an independent account of light perception in TKO mice.

Interestingly, in another mouse model combining genetic ablation of rods with the disabling of cone phototransduction ($Rho^{-/-}$, $Cnga3^{-/-}$) there is no detectable ERG response [17]. This strongly implicates residual rod function in the retained visual capabilities of TKO mice, which have the same cone mutation ($Cnga3^{-/-}$) but possess structurally intact rods ($Gnat1^{-/-}$). This is in line with a previous report of atypical rod function under cone-isolating conditions [63] and cautions the use of genetic deactivation without cell death in order to isolate melanopsin function [32]. Indeed, it could be that because rods play an important role in rodent visual acuity within the photopic range [11], the melanopsin system may in fact be potentiating a rod-

driven signal to allow pattern discrimination by the visual system of mice lacking both *Gnat1*$^{-/-}$ and *Cnga3*$^{-/-}$ [36].

In terms of a mechanism of action for atropine in enhancing light-mediated BLA, it seems likely that there is a combination of pupillary dilation to spatially increase retinal luminance and a direct action on retinal signal processing. Interestingly, this information may be processed in the brain independently of established nociceptive pathways, as atropine, applied topically to the eyes fails to alter light-evoked responses in the spinal trigeminal nucleus [43]. In line with our findings, another recent study also reports that atropine (in combination with phenylepherine) can enhance ERG b-wave amplitudes in C57 wildtype and retinal degenerate mice [64]. The ability of atropine to enhance retinal function has implications for the interpretation of data arising from a range of visual neuroscience studies that employ this drug prior to measuring visual function [12,63,65].

### Relevance of BLA in mice to human photophobia

Recently, the melanopsin system has been implicated in the circuitry by which light exacerbates the symptoms of migraine headache [42]. This study showed that patients with outer retinal degenerations consistently report migraine-associated photophobia. Using indirect evidence the authors propose a neural circuitry that involves information from mRGCs converging with trigemino-vascular signals in the lateral posterior thalamic nuclei before the integrated information is relayed up to cortical regions involved in pain processing.

Our results confirm that in retinal degenerate mice, melanopsin alone can drive a progressive behavioural aversion to light which is associated with activation of the visual and retrosplenial cortex. Both these structures are innervated to some extent by dura/light sensitive thalamic neurons [42]. In the context of behavioural aversion to light, our identification of melanopsin-driven c-Fos induction (Figure S1) in the retrosplenial cortex (RSC) is of particular interest because stimulation of this region in humans can cause autonomic responses linked to emotional processing [66]. The RSC is a posterior division of the cingulate cortex [67], a limbic structure which is active during the perception of photophobia in humans [44]. The established role of RSC in functions such as memory and navigation [68], together with its anatomical connectivity to structures such as the hippocampus and superior colliculus [69,70] make this an important structure to examine in future studies exploring melanopsin's role in emotional and cognitive processing, which are widely regarded to be interlinked [71].

### Conclusions

Melanopsin in isolation is capable of attributing emotional salience to light sufficient to produce an aversive behavioural response that potentiates over time. This finding has relevance to the understanding of how spatial movements may be integrated with diurnal sleeping patterns to control circadian behaviour. Given the potential role for melanopsin in human photophobia, the study of brain regions involved in assigning affective valence to luminance represents an interesting avenue for future research. Surprisingly, the use of atropine to examine the role of the PLR in BLA also revealed that light perception, sufficient to generate an aversive behavioural response can occur in TKO mice, lacking melanopsin, a PLR and proper rod/cone function. The reinstatement of BLA in ChR2-transfected TKO mice confirms that pupillary constriction is not a requirement for light aversion in rodents.

## Materials and Methods

### Animals

All procedures were conducted according to the Home Office (UK) regulations, under the Animals (Scientific Procedures) Act of 1986, and with local (UCL-Institute of Ophthalmology, London, UK) ethics committee approval.

Four types of mice were used, wildtype (WT), *rd/rd cl* (melanopsin only, MO) [14,31], melanopsin knockout (MKO) *Opn4*$^{-/-}$ [30] and triple knockout (TKO) *Opn4*$^{-/-}$;*Gnat1*$^{-/-}$;*Cnga3*$^{-/-}$ [49]. The WT and MO are congenic on the C3H/He strain, whilst the MKO and TKO are a C57 BL6/129 mixed strain background. All animals were housed under a 12:12 light dark cycle, with food and water available *ad libitum*.

### Pupillometry

The PLR was measured in un-anaesthetised mice dark adapted for at least 1 hour. An infra-red light source was used to illuminate the left eye and frames were taken using a 12 bit SMD (1M60) digital camera mounted on top of a Leica MZ75 microscope using a magnification of 1. A long pass filter was interposed between the microscope lens and the mouse eye to block any light of less than 665 nm wavelength. The left eye was stimulated with broad-spectrum light originating from a xenon-arc lamp (Lambda DG-4, Linton Instrumentation) synchronized with the image capture using an electronic shutter (Melles-Griot). Short-pass and neutral density filters (Edmund Optics Ltd., York, UK) were combined to abolish stimulus light wavelengths above 600 nm. The light was then guided with a fibre optic through a light diffuser placed 2 cm away from the left eye stimulating with white light of 600 $\mu W/cm^2$ irradiance. The eye was stimulated for 24 seconds while collecting spatially binned (2×2) frames of the eye at 4 Hz. The pupil area was estimated off-line at each frame by an observer using customized MATLAB software and the results were downsampled to 1 Hz. Pupillometry was carried out on n = 5 TKO, n = 3 MO, and n = 4 TKO mice treated with AAV-*ChR2V*. One day after PLR assessment of the TKO and MO the same mice had bilateral application of atropine sulphate, 1%, (Minims, preservative free) under dim red light. After 1 hour of dark adaptation recording of their PLR was made as described above.

### Testing of open field light aversion behaviour

Adult mice (~100–250 days of age) of mixed sexes were used. We chose to use mice naïve to the experimental arena because although habituation is used in some light/dark choice protocols [72] this can reduce the amount of time spent in the dark [73] which may mask subtle light responses. The open field arena is shown in Figure 1A. The arena is square (26×26 cm) and is divided in half into an open front-half (FH) and an enclosed back-half (BH), with a small door through which the mouse can enter the enclosed area. The FH of the arena was either illuminated (light FH) or remained in darkness (dark FH) with a light-impervious cloth used to baffle the arena from stray sources of light. White light illumination was provided by a Philips Energy Light (Philips, Guildford UK) suspended 0.75 m above the whole arena (irradiance at floor level 600 $\mu W/cm^2$ or ~1300 Lux). The illumination did not cause a measurable change in temperature in the FH of the arena compared to the BH, as measured using heat probes. Air conditioning in the room served to regulate the temperature and also produced background white noise.

Only naïve animals were tested, that did not have previous exposure to the arena. All tests were carried out during the light phase (ZT1-11) of their light:dark cycle, and all animals were light adapted. At the start of each trial, each mouse was placed in the

FH of the arena under dim red illumination (after which this red light was turned off) and left for 30 minutes with either illumination or darkness in the FH. The time spent in each compartment was monitored using TRUSCAN (Coulburn Instruments, Inc Allentown, PA). After each trial the arena was thoroughly washed and then wiped with 70% ethanol and dried.

Some animals were treated with atropine prior to being tested in the arena. Here, animals were taken from their holding room, to a separate procedure room where 1 drop of atropine sulphate, 1%, (Minims, preservative free) was applied bilaterally, and the animals were then left in their home cage for at least 0.5–2 hours prior to being tested in a separate procedure room containing the open field arena.

Animals that did not enter the BH of the arena within the first 5 minutes of a trial were discounted from the analysis. Total numbers tested and those discounted are shown in table S1. In general, most animals entered the BH within the first couple of minutes and, in terms of latency to enter the BH, no significant differences between the genotypes or between different illuminations (light vs. darkness) were found (data not shown).

## Bilateral intraocular axotomy procedure

For axotomy surgery, triple knockout mice were deeply anaesthetized with a mixture of medetomidine hydrochloride (1 mg/kg) (Domitor, Pfizer, Kent, UK) and ketamine (75 mg/kg) and placed securely in a nose bar with eyes covered in ViscoTears (Novartis Pharmaceuticals UK Ltd). An ophthalmic operating microscope (Olympus) was used to visualize the optic nerve head directly through a glass coverslip before gripping the extra-ocular muscles with a pair of fine-toothed microsurgical tweezers (FST) and inserting a 30-gauge needle (attached to a 2.5 µl Hamilton syringe) through the sclera, directly into the sub-retinal space. This technique uses the same needle and sub-retinal approach that is routinely employed in cell transplantation studies [74]. Once the needle was sub-retinal and adjacent to the optic nerve head, the optic nerve (together with the central retinal artery) was easily severed using a swift back and forth movement. This surgical procedure is summarized in Figure 5A (in a schematic adapted from May and Lutjen-Drecoll, 2002 [75]). At the time of surgery, axotomy was confirmed by injecting 2 µl of saline to produce a retinal detachment beneath the successfully severed optic nerve head.

Following bilateral axotomy surgery, all animals were given an intra-peritoneal injection of the analgesic carprofen 5 mg/kg (Rimadyl, Pfizer, Kent, UK) and recovered with the anaesthetic antidote atipamezole 0.5 mg/kg (Anti-sedan Pfizer, Kent, UK). Animals had recovered well by the following morning and were run in the light aversion assay 8 days post-surgery. One day following the completion of behavioural testing, all mice were perfused and their brains processed for calretinin immunohistochemistry. In addition to the axotomised mice, for the purposes of comparison, several age-matched untreated TKOs (n = 3) were also perfused and their brains processed for calretinin immunohistochemistry. The anatomical positioning of brain sections was determined using the mouse brain atlas [76]. The calcium binding protein calretinin is expressed ubiquitously in retinal ganglion cell axons and is a well-characterised marker for assessing deafferentation of subcortical retino-recipient structures in the rodent [77]. Previous work in the rat [78] and mouse [79] has demonstrated that calretinin-positive axonal fibres in the superficial layers of superior colliculus originate exclusively from retinal ganglion cells and that these fibres are lost 7 days following successful optic nerve section.

## AAV vector injection

The preparation of the adeno-associated viral (AAV) vector used here has been described in detail previously [57]. In brief, it contains a *Channelrhodopsin-2/Venus* (*ChR2V*) fusion gene under the control of a hybrid cytomegalovirus/chicken β actin promoter. Four TKO adult mice (162 day-old) underwent bilateral intravitreal injections of the AAV2-*ChR2V* viral vector suspension ($1\times10^{12}$ particles/ml, measured by an ELISA assay as described previously [80]).

Mice were anaesthetised as above and the head stabilised in a nose-bar before inserting a 30-gauge needle (attached to a 2.5 µl Hamilton syringe) into the vitreous cavity. A total volume of 2 µl of the viral vector suspension was injected into each eye, followed by a parasentesis counter-injection made below the *ora serrata* (to relieve intraocular pressure). The mice were recovered as described above and tested two-months post-surgery for photophobic behaviour and pupillometry. Finally, they were perfused and the eyes processed for immunohistochemistry, with one retina from each animal removed and processed as a flat mount whilst the other was cryprotected, frozen and sectioned.

## Electroretinogram recordings

Experimentation was performed under dim red light (<0.25 µW/cm$^2$, >650 nm), and mice were long-term dark adapted (>12 hr) prior to recording. To compare the effects of atropine on the TKO ERG, mice were divided into two groups: 5 mice received atropine sulphate eye drops (1%; minims, preservative free) in each eye 30 minutes prior to recording, and 5 mice received no drops. Mice were initially anaesthetised with intra-peritoneal ketamine (70 mg/kg) and xylazine (7 mg/kg), which was maintained with an injection of subcutaneous ketamine (72 mg/ml) and xylazine (5 mg/ml).

Hypromellose solution (0.5%; Alcon Laboratories, Ltd., UK) was applied to each eye to retain corneal moisture and to provide sufficient adherence of a contact lens electrode to the corneal surface. A silver wire bite bar provided head support and acted as a ground, and a needle reference electrode (Ambu® Neuroline) was inserted approximately 5 mm from the base of contralateral eye, sufficiently distal to exclude signal interference. Electrodes were connected to a Windows PC via a signal conditioner (Model 1902 Mark III, CED, UK), which differentially amplified (x3000) and filtered (band-pass filter cut-off 0.5 to 200 Hz) the signal, and a digitizer (Model 1401, CED). Throughout experimentation, core body temperature was maintained at ~37°C via a homeothermic heat mat (Harvard Apparatus, Kent, UK). For ten minutes prior to first recordings, electrode stability was monitored; electrodes displaying any baseline instability were rejected.

A xenon arc source (Cairn Research Ltd., Kent, UK) connected to a ganzfeld sphere provided white light flashes with a peak corneal irradiance of 1.58 mW/cm$^2$ (2370 Lux). A series of 15 ms flashes were applied using an electrically controlled mechanical shutter (Cairn Research Ltd.) with a 40 s interstimulus interval. An average ERG response was generated from 25 flashes, and the b-wave amplitude measured (from a-wave peak to b-wave peak) and compared statistically.

## Immunohistochemistry

Animals were deeply anaesthetised with sodium pentobarbital (60 mg/kg) and then perfused with 0.1 M PBS followed by 4% paraformaldehyde (in 0.1 M phosphate buffer), with overnight post-fixation at 4°C. Tissues to be cryostat sectioned were cryoprotected overnight at 4°C in 30% sucrose solution (in 0.1 M PBS), and then frozen with a dry ice/acetone slurry. Coronal brain sections (30 µm thick) were cut on the cryostat and

processed free-floating, while retinal sections were cryosectioned (14 μm thick) and mounted onto Superfrost Plus slides (BDH, Poole, UK).

Tissues were blocked for 2 h with 5% normal donkey serum (NDS) in PBS containing 0.3% (retinal/brain sections) or 3% (flat mounts) Triton X-100 (PBS-TX). The tissue was subsequently incubated overnight in PBS-TX containing 1% NDS and either a goat primary antibody raised against calretinin (1:1000, Swant, Bellinzona, Switzerland) or a rabbit anti-β galactosidase antibody (1:5,000, Abcam, Cambridge, UK). Following washes in PBS, tissue was incubated for 2 h in PBS-TX containing 2% NDS and an appropriate TRITC-labelled secondary antibody (1:200, Jackson ImmunoReseach, West Grove, PA). Tissue was washed extensively in PBS and TRIS buffer. Cell nuclei were counter-stained with DAPI (1:5,000 Sigma) before cover-slipping with Vectashield (Vector Laboratories, Burlingame, CA). Fluorescence labelling was examined using a Zeiss confocal microscope (with LSM Image Browser software, Welwyn Garden City, UK).

### Statistical Analysis

All data was analysed using GraphPad Prism software (GraphPad Software, San Diego, CA). Prior to analysis by Student's *t*-tests or ANOVA the proportional light aversion data were transformed Y = Arcsine(Y). One-tailed Student's *t*-tests were used to analyse both the effect of light on the total amount of time spent in the dark BH (light FH versus dark FH) over the whole 30-minute trial, and also the electroretinogram b-wave data. To analyse the effect of rods and cones, light aversion behaviour was compared between the congenic WT and MO by two-way ANOVA (factors: genotype and light) followed by Bonferroni's multiple comparison tests. To analyse the effect of atropine a two-way ANOVA (factors: light and atropine) was performed followed by Bonferroni's multiple comparison tests. The effect of light over the duration of the trial was investigated by using both regression analysis and two-way repeated measures ANOVA (RM ANOVA), factors: light and duration of the trial, (subjects were significantly matched in all cases $p<0.0001$) this was followed by Bonferroni post-tests with light FH versus dark FH at each time point in the trial.

## Supporting Information

**Figure S1 Light induced c-fos in the visual and retrosplenial cortex (RSC) of MO (*rd/rd cl*) mice.** Images on the left are from an animal that remained in the dark whilst those on the right from an animal that was exposed to light. Nuclei positive for the immediate early gene c-Fos are green, whilst neurofilament-H (NF-H) is in red. (**A**) Montage of the cortex, −3.52 mm from the Bregma, Scale bar 400 μm. (**B**) Higher magnification of the medial visual cortex (V1/2) clearly showing light induced neural activity in layers II–VI. (**C**) Higher magnification of the retroplenial cortex showing light induced c-Fos, (**B–C**) Scale bars 200 μm. Methods: Mice (n = 3 per condition) were dark-adapted overnight and at 07:00, still in their home cages, either exposed to 1.5 hours of ~1300 lux white light or maintained in darkness. They were then perfused and brain sections processed for immunohistochemistry as described in the main text using rabbit anti-c-fos (PC38, Calbiochem, 1:5,000) and mouse anti-neurofilament heavy chain (SMI-32, Covance, 1:5,000) followed by secondaries antibodies (FITC anti-rabbit IgG and TRITC anti-mouse IgG, both from Jackson ImmunoReseach, West Grove, PA). The neurofilament-H antibody was used to match up sections using cytoarchitectural boundaries in the cortex, as described previously by Van der Gucht *et al.*, 2007. (TIF)

**Figure S2 Behavioural light aversion in old versus young MO (*rd/rd cl*) mice.** (**A**) The amount of time old animals (394±46 day-old; mean±SD) spend in the dark back-half (BH) during the 30-min trial is not significantly different to the amount of time spent there by younger animals (166±6 day-old), although the average time that the old animals spend in the dark is slightly higher (~58% versus ~46%). (**B**) Over the course of the trial it is revealed that the old animals spend significantly more time (~70%) in the dark than the younger animals during the first 5 minutes of the trial (Two-way repeated measures ANOVA demonstrates: (1) a significant interaction ($p<0.05$) aging X duration of the trial and (2) a significant effect of duration ($p<0.05$), Bonferonni post-tests show that in the first 5 minutes the old animals spend significantly more time in the dark ($p<0.01$) than younger animals). It seems unlikely that this is due to poorer mobility in the old animals as they continued to move around the arena sampling both light and dark regions for the rest of the trial. Due to this behaviour during the first 5-minutes there is no longer a significant positive correlation of photophobic behaviour in the old animals, they continue spending a similar proportion of their time in the dark BH throughout the 30 minutes. Abbreviations: BH, back-half; MO, melanopsin only. (TIF)

**Figure S3 Calretinin positive retinal-afferents (red) are lost 9 days post axotomy in the olivary pretectal nucleus (OPT) and the optic chiasm (och) of TKO mice.** Compare **A** with **B** for the OPT and **C** with **D** for the och. Brain sections from equivalent Bregma positions were imaged in control and axotomised brains as indicated in **A** for the OPT and in **C** for the och. Scale bar in D for all plates is 100 μm. Abbreviations: oc, optic chiasm; OPT, olivary pretectal nucleus; TKO, triple knockout. (TIF)

**Figure S4 Pupillometry in triple knockout (TKO) mice following transduction of the inner retina with Channelrhodopsin 2/Venus fusion protein.** At two-months post-introduction of the AAV2-*ChR2V* the pupillary light reflex has not been re-instated in these animals. (TIF)

**Table S1** (DOC)

## Acknowledgments

We gratefully acknowledge the kind help and assistance of Prof. Rob Lucas from the University of Manchester. We also thank Prof. Russell G. Foster of Oxford University for providing *rd/rd cl* mice. We wish to acknowledge the technical assistance of Matthew Smart and Shazeen Hasan.

## Author Contributions

Conceived and designed the experiments: MS PJC AAV. Performed the experiments: MS CG AA AEA JML AAV. Analyzed the data: MS CG AEA. Contributed reagents/materials/analysis tools: ES HT. Wrote the paper: AAV MS.

## References

1. Crozier WJ, Pincus G (1927) Phototropism in Young Rats. J Gen Physiol 10: 407–417.
2. Keller FS (1941) Light aversion in the white rat. Psychological Record 4: 235–250.
3. Welker WI (1959) Escape, exploratory, and food-seeking responses of rats in a novel situation. J Comp Physiol Psychol 52: 106–111.
4. Flynn JP, Jerome EA (1952) Learning in an automatic multiple-choice box with light as incentive. J Comp Physiol Psychol 45: 336–340.

5. Crawley J, Goodwin FK (1980) Preliminary report of a simple animal behavior model for the anxiolytic effects of benzodiazepines. Pharmacol Biochem Behav 13: 167–170.
6. Misslin R, Belzung C, Vogel E (1989) Behavioural validation of a light/dark choice proceedure for testing anti-anxiety agents. Behavioural Process 18: 119–132.
7. Bourin M, Hascoet M (2003) The mouse light/dark box test. Eur J Pharmacol 463: 55–65.
8. Recober A, Kaiser EA, Kuburas A, Russo AF (2010) Induction of multiple photophobic behaviors in a transgenic mouse sensitized to CGRP. Neuropharmacology 58: 156–165.
9. Russo AF, Kuburas A, Kaiser EA, Raddant AC, Recober A (2009) A Potential Preclinical Migraine Model: CGRP-Sensitized Mice. Mol Cell Pharmacol 1: 264–270.
10. Altman J (1962) Effects of lesions in central nervous visual structures on light aversion of rats. Am J Physiol 202: 1208–1210.
11. Schmucker C, Seeliger M, Humphries P, Biel M, Schaeffel F (2005) Grating acuity at different luminances in wild-type mice and in mice lacking rod or cone function. Invest Ophthalmol Vis Sci 46: 398–407.
12. Guler AD, Ecker JL, Lall GS, Haq S, Altimus CM, et al. (2008) Melanopsin cells are the principal conduits for rod-cone input to non-image-forming vision. Nature 453: 102–105.
13. Provencio I, Rollag MD, Castrucci AM (2002) Photoreceptive net in the mammalian retina. This mesh of cells may explain how some blind mice can still tell day from night. Nature 415: 493.
14. Lucas RJ, Freedman MS, Munoz M, Garcia-Fernandez JM, Foster RG (1999) Regulation of the mammalian pineal by non-rod, non-cone, ocular photoreceptors. Science 284: 505–507.
15. Freedman MS, Lucas RJ, Soni B, von Schantz M, Munoz M, et al. (1999) Regulation of mammalian circadian behavior by non-rod, non-cone, ocular photoreceptors. Science 284: 502–504.
16. Berson DM, Dunn FA, Takao M (2002) Phototransduction by retinal ganglion cells that set the circadian clock. Science 295: 1070–1073.
17. Barnard AR, Appleford JM, Sekaran S, Chinthapalli K, Jenkins A, et al. (2004) Residual photosensitivity in mice lacking both rod opsin and cone photoreceptor cyclic nucleotide gated channel 3 alpha subunit. Vis Neurosci 21: 675–683.
18. Goz D, Studholme K, Lappi DA, Rollag MD, Provencio I, et al. (2008) Targeted destruction of photosensitive retinal ganglion cells with a saporin conjugate alters the effects of light on mouse circadian rhythms. PLoS ONE 3: e3153.
19. Hetherington L, Benn M, Coffey PJ, Lund RD (2000) Sensory capacity of the royal college of surgeons rat. Invest Ophthalmol Vis Sci 41: 3979–3983.
20. Lin B, Koizumi A, Tanaka N, Panda S, Masland RH (2008) Restoration of visual function in retinal degeneration mice by ectopic expression of melanopsin. Proc Natl Acad Sci U S A 105: 16009–16014.
21. Mrosovsky N, Hampton RR (1997) Spatial responses to light in mice with severe retinal degeneration. Neurosci Lett 222: 204–206.
22. Jimenez AJ, Garcia-Fernandez JM, Gonzalez B, Foster RG (1996) The spatiotemporal pattern of photoreceptor degeneration in the aged rd/rd mouse retina. Cell Tissue Res 284: 193–202.
23. Garcia-Fernandez JM, Jimenez AJ, Foster RG (1995) The persistence of cone photoreceptors within the dorsal retina of aged retinally degenerate mice (rd/rd): implications for circadian organization. Neurosci Lett 187: 33–36.
24. Punzo C, Kornacker K, Cepko CL (2009) Stimulation of the insulin/mTOR pathway delays cone death in a mouse model of retinitis pigmentosa. Nat Neurosci 12: 44–52.
25. Lin B, Masland RH, Strettoi E (2009) Remodeling of cone photoreceptor cells after rod degeneration in rd mice. Exp Eye Res 88: 589–599.
26. Isoldi MC, Rollag MD, Castrucci AM, Provencio I (2005) Rhabdomeric phototransduction initiated by the vertebrate photopigment melanopsin. Proc Natl Acad Sci U S A 102: 1217–1221.
27. Panda S, Nayak SK, Campo B, Walker JR, Hogenesch JB, et al. (2005) Illumination of the melanopsin signaling pathway. Science 307: 600–604.
28. Mrosovsky N, Lucas RJ, Foster RG (2001) Persistence of masking responses to light in mice lacking rods and cones. J Biol Rhythms 16: 585–588.
29. Lucas RJ, Douglas RH, Foster RG (2001) Characterization of an ocular photopigment capable of driving pupillary constriction in mice. Nat Neurosci 4: 621–626.
30. Lucas RJ, Hattar S, Takao M, Berson DM, Foster RG, et al. (2003) Diminished pupillary light reflex at high irradiances in melanopsin-knockout mice. Science 299: 245–247.
31. Lupi D, Oster H, Thompson S, Foster RG (2008) The acute light-induction of sleep is mediated by OPN4-based photoreception. Nat Neurosci 11: 1068–73.
32. Altimus CM, Guler AD, Villa KL, McNeill DS, Legates TA, et al. (2008) Rods-cones and melanopsin detect light and dark to modulate sleep independent of image formation. Proc Natl Acad Sci U S A 105: 19998–20003.
33. Tsai JW, Hannibal J, Hagiwara G, Colas D, Ruppert E, et al. (2009) Melanopsin as a sleep modulator: circadian gating of the direct effects of light on sleep and altered sleep homeostasis in Opn4(−/−) mice. PLoS Biol 7: e1000125.
34. Mrosovsky N, Salmon PA (2002) Learned arbitrary responses to light in mice without rods or cones. Naturwissenschaften 89: 525–527.
35. Hattar S, Kumar M, Park A, Tong P, Tung J, et al. (2006) Central projections of melanopsin-expressing retinal ganglion cells in the mouse. J Comp Neurol 497: 326–349.
36. Ecker JL, Dumitrescu ON, Wong KY, Alam NM, Chen SK, et al. (2010) Melanopsin-Expressing Retinal Ganglion-Cell Photoreceptors: Cellular Diversity and Role in Pattern Vision. Neuron 67: 49–60.
37. Dacey DM, Liao HW, Peterson BB, Robinson FR, Smith VC, et al. (2005) Melanopsin-expressing ganglion cells in primate retina signal colour and irradiance and project to the LGN. Nature 433: 749–754.
38. Zaidi FH, Hull JT, Peirson SN, Wulff K, Aeschbach D, et al. (2007) Short-wavelength light sensitivity of circadian, pupillary, and visual awareness in humans lacking an outer retina. Curr Biol 17: 2122–2128.
39. Drummond PD (1986) A quantitative assessment of photophobia in migraine and tension headache. Headache 26: 465–469.
40. Lebensohn J (1934) The nature of photophobia. Archives of Ophthalmology 12: 380–390.
41. Lebensohn JE (1951) Photophobia: mechanism and implications. Am J Ophthalmol 34: 1294–1300.
42. Noseda R, Kainz V, Jakubowski M, Gooley JJ, Saper CB, et al. (2010) A neural mechanism for exacerbation of headache by light. Nat Neurosci 13: 239–245.
43. Okamoto K, Tashiro A, Chang Z, Bereiter DA (2010) Bright light activates a trigeminal nociceptive pathway. Pain 149: 235–242.
44. Moulton EA, Becerra L, Borsook D (2009) An fMRI case report of photophobia: activation of the trigeminal nociceptive pathway. Pain 145: 358–363.
45. King V (1972) Discomfort glare from flashing sources. J Am Optom Assoc 43: 53–56.
46. Stringham JM, Fuld K, Wenzel AJ (2004) Spatial properties of photophobia. Invest Ophthalmol Vis Sci 45: 3838–3848.
47. Sliney DH (1997) Ocular exposure to environmental light and ultraviolet—the impact of lid opening and sky conditions. Dev Ophthalmol 27: 63–75.
48. Stringham JM, Fuld K, Wenzel AJ (2003) Action spectrum for photophobia. J Opt Soc Am A Opt Image Sci Vis 20: 1852–1858.
49. Hattar S, Lucas RJ, Mrosovsky N, Thompson S, Douglas RH, et al. (2003) Melanopsin and rod-cone photoreceptive systems account for all major accessory visual functions in mice. Nature 424: 76–81.
50. Van der Gucht E, Hof PR, Van Brussel L, Burnat K, Arckens L (2007) Neurofilament protein and neuronal activity markers define regional architectonic parcellation in the mouse visual cortex. Cereb Cortex 17: 2805–2819.
51. Semo M, Lupi D, Peirson SN, Butler JN, Foster RG (2003) Light-induced c-fos in melanopsin retinal ganglion cells of young and aged rodless/coneless (rd/rd cl) mice. Eur J Neurosci 18: 3007–3017.
52. Semo M, Peirson S, Lupi D, Lucas RJ, Jeffery G, et al. (2003) Melanopsin retinal ganglion cells and the maintenance of circadian and pupillary responses to light in aged rodless/coneless (rd/rd cl) mice. Eur J Neurosci 17: 1793–1801.
53. Reader AL, 3rd (1977) Mydriasis from Datura wrightii. Am J Ophthalmol 84: 263–264.
54. Allen AE, Cameron MA, Brown TM, Vugler AA, Lucas RJ (2010) Visual responses in mice lacking critical components of all known retinal phototransduction cascades. PLoS ONE 10.1371/journal.pone.0015063.
55. Lau KC, So KF, Campbell G, Lieberman AR (1992) Pupillary constriction in response to light in rodents, which does not depend on central neural pathways. J Neurol Sci 113: 70–79.
56. Robinson GA, Madison RD (2004) Axotomized mouse retinal ganglion cells containing melanopsin show enhanced survival, but not enhanced axon regrowth into a peripheral nerve graft. Vision Res 44: 2667–2674.
57. Tomita H, Sugano E, Yawo H, Ishizuka T, Isago H, et al. (2007) Restoration of visual response in aged dystrophic RCS rats using AAV-mediated channelopsin-2 gene transfer. Invest Ophthalmol Vis Sci 48: 3821–3826.
58. Tomita H, Sugano E, Isago H, Hiroi T, Wang Z, et al. (2010) Channelrhodopsin-2 gene transduced into retinal ganglion cells restores functional vision in genetically blind rats. Exp Eye Res 90: 429–436.
59. Tian N, Copenhagen DR (2003) Visual stimulation is required for refinement of ON and OFF pathways in postnatal retina. Neuron 39: 85–96.
60. Hannibal J, Fahrenkrug J (2004) Melanopsin containing retinal ganglion cells are light responsive from birth. Neuroreport 15: 2317–2320.
61. Misslin R, Cirang M (1986) Does neophobia necessarily imply fear or anxiety. Behavioural Processes 12: 45–50.
62. Berson DM, Castrucci AM, Provencio I (2010) Morphology and mosaics of melanopsin-expressing retinal ganglion cell types in mice. J Comp Neurol 518: 2405–2422.
63. Seeliger MW, Grimm C, Stahlberg F, Friedburg C, Jaissle G, et al. (2001) New views on RPE65 deficiency: the rod system is the source of vision in a mouse model of Leber congenital amaurosis. Nat Genet 29: 70–74.
64. Mojumder DK, Wensel TG (2010) Topical mydriatics affect light-evoked retinal responses in anesthetized mice. Invest Ophthalmol Vis Sci 51: 567–576.
65. Hubel DH, Wiesel TN (1962) Receptive fields, binocular interaction and functional architecture in the cat's visual cortex. J Physiol 160: 106–154.
66. MacLean P (1949) Psychosomatic disease and the visceral brain; recent developments bearing on the Papez theory of emotion. Psychosom Med 11: 338–353.
67. Papez J (1937) A proposed mechanism of emotion. Arch Neurol Psychiatry 38: 725–734.
68. Vann SD, Aggleton JP, Maguire EA (2009) What does the retrosplenial cortex do? Nat Rev Neurosci 10: 792–802.
69. Garcia Del Cano G, Gerrikagoitia I, Martinez-Millan L (2000) Morphology and topographical organization of the retrospleniocollicular connection: a pathway

to relay contextual information from the environment to the superior colliculus. J Comp Neurol 425: 393–408.
70. Wyss JM, Van Groen T (1992) Connections between the retrosplenial cortex and the hippocampal formation in the rat: a review. Hippocampus 2: 1–11.
71. Ochsner KN, Phelps E (2007) Emerging perspectives on emotion-cognition interactions. Trends Cogn Sci 11: 317–318.
72. Thiels E, Hoffman EK, Gorin MB (2008) A reliable behavioral assay for the assessment of sustained photophobia in mice. Curr Eye Res 33: 483–491.
73. Onaivi ES, Martin BR (1989) Neuropharmacological and physiological validation of a computer-controlled two-compartment black and white box for the assessment of anxiety. Prog Neuropsychopharmacol Biol Psychiatry 13: 963–976.
74. Vugler A, Carr AJ, Lawrence J, Chen LL, Burrell K, et al. (2008) Elucidating the phenomenon of HESC-derived RPE: anatomy of cell genesis, expansion and retinal transplantation. Exp Neurol 214: 347–361.
75. May CA, Lutjen-Drecoll E (2002) Morphology of the murine optic nerve. Invest Ophthalmol Vis Sci 43: 2206–2212.
76. Paxinos G, Franklin K (2001) The mouse brain in stereotaxic coordinates. San Diego.
77. Vugler AA, Coffey PJ (2003) Loss of calretinin immunoreactive fibers in subcortical visual recipient structures of the RCS dystrophic rat. Exp Neurol 184: 464–478.
78. Arai M, Arai R, Sasamoto K, Kani K, Maeda T, et al. (1993) Appearance of calretinin-immunoreactive neurons in the upper layers of the rat superior colliculus after eye enucleation. Brain Res 613: 341–346.
79. Gobersztejn F, Britto LR (1996) Calretinin in the mouse superior colliculus originates from retinal ganglion cells. Braz J Med Biol Res 29: 1507–1511.
80. Sugano E, Tomita H, Ishiguro S, Abe T, Tamai M (2005) Establishment of effective methods for transducing genes into iris pigment epithelial cells by using adeno-associated virus type 2. Invest Ophthalmol Vis Sci 46: 3341–3348.

Neuroscience Research 69 (2011) 223–233

Contents lists available at ScienceDirect

Neuroscience Research

journal homepage: www.elsevier.com/locate/neures

# Lineage analysis of newly generated neurons in organotypic culture of rat hippocampus

Jun Yokose[a,b,c], Toru Ishizuka[a,b], Takeshi Yoshida[d], Jun Aoki[d], Yoshio Koyanagi[d], Hiromu Yawo[a,b,c,e,*]

[a] Department of Developmental Biology and Neuroscience, Tohoku University Graduate School of Life Sciences, Sendai 980-8577, Japan
[b] JST, CREST, Tokyo 102-0075, Japan
[c] Tohoku University Basic and Translational Research Center for Global Brain Science, Sendai 980-8575, Japan
[d] Laboratory of Viral Pathogenesis, Institute for Virus Research, Kyoto University, Kyoto 606-8507, Japan
[e] Center for Neuroscience, Tohoku University Graduate School of Medicine, Sendai 980-8575, Japan

ARTICLE INFO

*Article history:*
Received 16 August 2010
Received in revised form 8 November 2010
Accepted 26 November 2010
Available online 8 December 2010

*Keywords:*
Postnatal neurogenesis
Hippocampus
Slice culture
Retrovirus
Lineage
Differentiation
Programmed cell death
Critical period

ABSTRACT

New neurons are continuously generated in the hippocampus at the subgranular zone of the dentate granule cell layer throughout life. However, the lineage of newly generated neurons is unknown in detail. Here, using a retrovirus vector encoding EGFP, we labeled proliferating cells in an organotypic slice culture of the postnatal hippocampus of rat, and tracked their descendents over a long period. At 28 days post-inoculation, the phenotypes of the cells were immunohistochemically identified using specific antibodies to cell-type markers such as HuC/D (pan-neuronal marker), GFAP (astrocyte marker), Prox1 (dentate granule cell marker) or NeuN (mature neuronal marker). We found that the cells were mostly GFAP-negative in the HuC/D-positive lineages. The EGFP-expressing cells were often untraceable shortly after cell division in the HuC/D-positive lineages. The postmitotic periods of these cells distributed between 2 and 14 days. For the lineages expressing both Prox1 and NeuN the newborn cells became untraceable in a similar period (2–10 days). It is suggested that the newly generated neurons differentiate to mature dentate granule cells in the slice culture once they have survived over this critical traceability period.


## 1. Introduction

New neurons are continuously generated postnatally in the hippocampus of mammals including humans (Altman and Das, 1965; Cameron et al., 1993; Eriksson et al., 1998). When the new neurons generated in the subgranular zone (SGZ) of the dentate gyrus differentiate into functional dentate granule cell layer (GCL) neurons, they are integrated into the hippocampal circuitry for certain forms of memory such as spatial relation memory and/or contextual fear conditioning, although some findings remain controversial (Bruel-Jungerman et al., 2006; Meshi et al., 2006; Saxe et al., 2006; Dupret et al., 2008; Imayoshi et al., 2008; Zhang et al., 2008; see reviews by Aimone et al., 2006; Lledo et al., 2006; Kempermann, 2008). In the postnatal hippocampus, neurogenesis is a multi-step process consisting of the division of a putative stem/precursor cell (type-1 cell), the transient amplification of putative progenitor cells (type-2, -3 cells), the selection of surviving cells and their differentiation into functional neurons (Kempermann et al., 2004). The stem cells could be multi-potent with the ability to generate neurons, astrocytes and oligodendrocytes (Palmer et al., 1997). On the other hand, the type-2, -3 cells are thought to be destined to generate neurons since these cells are positive for immature neuronal marker proteins such as doublecortin and PSA-NCAM as well as for membrane properties reminiscent of immature neurons (Brown et al., 2003; Fukuda et al., 2003; Filippov et al., 2003; Kronenberg et al., 2003). The multi-potent precursor cells transform to the neuron-destined cells early during the type-2 cell stage (Steiner et al., 2006). Every step has been presumed to be under the regulation of various neurogenic stimuli. For example, voluntary movements such as the wheel running, facilitate the proliferation of transiently amplifying progenitor cells, whereas environmental enrichment may facilitate the survival of the final descendents (Kempermann et al., 1997; van Praag et al., 1999; Kronenberg et al., 2003; Bruel-Jungerman et al., 2005; Steiner et al., 2006, 2008). To further investigate how the proliferation and the survival are regulated, the lineage has to be followed up for an individual progenitor

*Abbreviations:* DIV, days *in vitro*; DPI, days post-inoculation; RV, retrovirus vector.

* Corresponding author at: Department of Developmental Biology and Neuroscience, Tohoku University Graduate School of Life Sciences, 2-1-1 Katahira, Aoba-ku, Sendai 980-8577, Japan. Tel.: +81 22 217 6208; fax: +81 22 217 6211.
*E-mail addresses:* a9bd2009@s.tohoku.ac.jp (J. Yokose), ishizuka@m.tohoku.ac.jp (T. Ishizuka), koegadekaina@ybb.ne.jp (T. Yoshida), quizmaster0918@yahoo.co.jp (J. Aoki), ykoyanag@virus.kyoto-u.ac.jp (Y. Koyanagi), yawo-hiromu@m.tohoku.ac.jp (H. Yawo).

0168-0102/$ – see front matter © 2010 Elsevier Ireland Ltd and the Japan Neuroscience Society. All rights reserved.
doi:10.1016/j.neures.2010.11.010

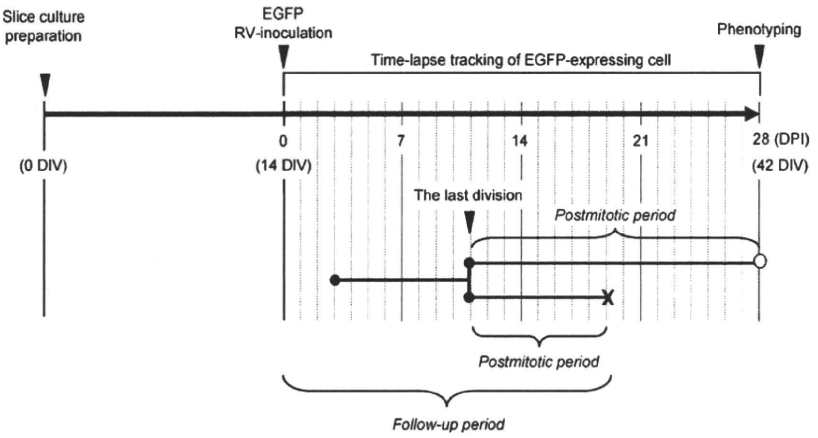


**Fig. 1.** Experimental protocol of lineage analysis. The newly generated cells and their descendents were followed after the inoculation of the retrovirus vector (RV) encoding EGFP. Their phenotypes were determined immunohistochemically at 28 days post-inoculation (DPI). The follow-up period was measured from the date of retrovirus vector inoculation in DPI. The postmitotic period was measured from the last division to the time of interest.

cell since the onset of each key process of neurogenesis occurs asynchronously.

Although the neurogenic processes have been extensively studied using animal model systems *in vivo*, it appears to be difficult to identify a single progenitor cell and to track its fate for a certain period. To solve this, here we used the organotypic slice culture of hippocampus as an *ex vivo* model preparation (Kamada et al., 2004; Raineteau et al., 2004; Laskowski et al., 2005; Poulsen et al., 2005). In the slice culture, the network is organized similar to that in living animals (Gähwiler, 1984; Zimmer and Gähwiler, 1984; Dailey et al., 1994) with a few rearrangements as a consequence of the afferent deprivation (Robain et al., 1994; Gutierrez and Heinemann, 1999) and the morphological and the physiological features of a neuron are similar to those in living animals (Stoppini et al., 1991; Okada et al., 1995; Gähwiler et al., 1997). Moreover, the newly generated cells can be directly observed under fluorescent microscopy (Kamada et al., 2004; Namba et al., 2007). In the present study, using retrovirus vectors, we labeled the newly generated cells with EGFP, investigated the lineage of individual progenitors for up to four weeks in the hippocampal slice culture and identified their phenotypes using HuC/D as a molecular marker of the neuron-generating lineage. The slice culture system enabled us to track a single progenitor cell and its descendents as a lineage in the postnatal hippocampus. Furthermore, the results indicate that the cells became often untraceable 2–14 days after cell division in the neuron-generating lineages.

## 2. Materials and methods

All animal experiments were approved by the Tohoku University Committee for Animal Experiments and were carried out in accordance with the Guidelines for Animal Experiments and Related Activities in Tohoku University as well as the guiding principles of the Physiological Society of Japan and the NIH.

### 2.1. Hippocampal slice culture

Hippocampal organotypic cultures were prepared from postnatal day 7 (P7) Wistar rats (Japan SLC Inc., Shizuoka, Japan) and cultured according to the standard interface method with some modifications (Stoppini et al., 1991; Sakaguchi et al., 1994; Kamada et al., 2004). Briefly, after decapitation the brain was removed, dissected and transversely sliced at the hippocampus into a 350 μm thickness on a McIlwain tissue chopper (The Mickle Laboratory Engineering, Guildford, Surrey, UK). In our experiments, slices were usually obtained from the dorsal part of rat hippocampus. The isolated slices were incubated on ice for at least 15–20 min in a solution containing (in mM) 236 mannitol, 3 KCl, 10 HEPES, 4 NaOH, 7 $MgCl_2$, 22 D-glucose, 1 kinurenic acid, penicillin and streptomycin (100 U/ml and 100 μg/ml, respectively), and were transferred onto porous membrane inserts (Millicell-CM: PICM03050, Millipore, Billerica, MA, USA). The slices were maintained in a humidified incubator at 34 °C in a 5% $CO_2$ atmosphere. The culture medium consisted of 50% OPTI-MEM (Invitrogen, Carlsbad, CA, USA), 25% heat-inactivated horse serum (Invitrogen) and 25% Hank's balanced salt solution (Invitrogen). It was further supplemented with D-glucose (5 g/L), penicillin (100 U/ml, Sigma–Aldrich, St. Louis, MO, USA) and streptomycin (100 μg/ml, Sigma–Aldrich), and was changed twice a week.

### 2.2. Retrovirus inoculation and time-lapse tracking of EGFP-expressing cells

Retroviral vectors encoding EGFP were prepared as described previously (Kamada et al., 2004) and their titers were $9 \times 10^6$ transduction U/ml. We reduced the amount of virus solution as little as possible so as the EGFP-expressing cells to be found in isolation. Typically, 0.1–0.2 μl of the solution containing these vectors was injected by at three positions in the suprapyramidal blade of the GCL in slices at 14 days *in vitro* (14 DIV), and the injected sites in the suprapyramidal region were daily observed (Fig. 1) under an inverted fluorescent microscope (Axiovert 200, Carl Zeiss, Göttingen, Germany) equipped with a 32× objective with long working distance (32×, LD A-Plan, Carl Zeiss). As only proliferating cells incorporate the transgene into their genome by the retroviral labeling method, newly generated cells and their descendants would specifically express EGFP. Once the EGFP-expressing cell was found in isolation, it was centered to the visual field and imaged at every two days for up to 28 days post-inoculation (28 DPI). The change of the visual field was kept to minimum during the tracking period by using several other fluorescent cells as landmarks. To prevent alkalization of the medium, the slices were kept in a humidified 5% $CO_2$/95% $O_2$ environment during imaging on the microscope. When the image clearly indicated division of the targeted cell, it was defined as the date of cell division. When a tracked cell was not found anywhere from top to bottom of the slice in the monitoring region (width ±295 μm; height ±394 μm) of the dentate gyrus, the cell was defined as "untraceable" because it could not be proven as having died. The first day of this detection was defined as the date of untraceability. At 28 DPI, the slices were fixed and subjected to immunohistochemistry as described below. Each new-

born cell and its descendents were tracked up to 28 DPI, identified their phenotypes and summarized as a cell lineage.

As shown in Fig. 1, the time measured from the date of retrovirus inoculation to that of untraceability was defined as the follow-up period. The time measured from the date of last division to that of untraceability was defined as the postmitotic period. The postmitotic period of a survived cell was measured as that between the last division and the phenotyping at 28 DPI, although this would be an underestimation.

### 2.3. Immunohistochemistry

Phenotypes of the newly generated EGFP-expressing cells were investigated immunohistochemically at 17 DIV (3 DPI) (42 slices, 230 cells) or at 42 DIV (28 DPI) (57 slices, 110 cells) using antibodies to Nestin, GFAP, HuC/D, Plox1 and NeuN in combination. Nestin is one of the intermediate filaments expressed specifically in neuroblasts and myoblasts (Lendahl et al., 1990) and a putative neural precursor marker (Ernst and Christie, 2005; Lagace et al., 2007). GFAP is a marker of non-neuronal cells (Seri et al., 2001) including terminally differentiated astrocytes (Goldman, 2003; Seri et al., 2004), radial glial cells, which have neurogenic potential (Seri et al., 2001), and type-1 neural progenitors (Kronenberg et al., 2003; Kamada et al., 2004). Members of Hu protein family have been identified as RNA-binding proteins that are expressed in both early postmitotic and mature neurons and are involved in the differentiation and/or the maintenance of neurons (Wakamatsu and Weston, 1997; Akamatsu et al., 2005). Prox1 is specifically expressed in mature GCL neurons and immature neurons that are differentiating to them (Alfonoso and Guillermo, 2007; Galeeva et al., 2007). NeuN is a specific marker of mature neurons.

Slices were fixed with 4% paraformaldehyde in 0.1 M sodium phosphate buffer (pH 7.2) at 4 °C for 30 min and then washed in PBS. After the slices were peeled off from the membrane, all subsequent incubations were carried out in free-floating mode in a dish. The slices were blocked in PBS including 5% normal donkey serum and 0.3% Triton X-100 at 4 °C overnight, then treated with the primary antibodies in PBS including 5% donkey serum and 0.3% Triton X-100 at 4 °C for 24 h. In a series of experiments the sample was triply labeled by the combination of the following primary antibodies: rabbit anti-EGFP IgG (1:1000; a generous gift from Drs. T. Kaneko and K. Nakamura, Kyoto University, Japan), rat anti-GFP IgG (1:2000; 04404-26, Nacalai tesque, Kyoto, Japan), guinea pig anti-GFAP IgG (1:1000; 03223, Advanced Immunochemical, Long Beach, CA, USA), mouse anti-HuC/D IgG ($IgG_{2b}$, 1:1000; A21271, Molecular probes, Eugene, OR, USA), rabbit anti-Prox1 IgG (1:2000; AB5475, Chemicon, Tamecula, CA, USA) and mouse anti-NeuN IgG (1:1000; MAB377, Chemicon). After washing four times (30 min each) at room temperature in PBS with 0.1% Triton X-100 the slices were incubated at room temperature for 5–6 h with the following secondary antibodies in PBS including 5% normal donkey serum and 0.3% Triton X-100: Alexa Fluor 488-, 647-conjugated donkey anti-mouse IgG, Alexa Fluor 488-, 546-conjugated donkey anti-rabbit IgG, Alexa Fluor 633-conjugated goat anti-rabbit IgG, Alexa Fluor 568-, 633-conjugated goat anti-Guinea pig IgG and Alexa Fluor goat 488-conjugated anti-rat IgG (1:200; all purchased from Molecular Probes).

For the triple labeling with two mouse monoclonal antibodies, we used the Zenon mouse IgG labeling kit with either Alexa Fluor 546 (Z25004, Molecular Probes) or 647 (Z25208, Molecular Probes). Anti-Nestin $IgG_1$ (1:1000; MAB353, Chemicon) or anti-HuC/D $IgG_{2b}$ (1:200) was incubated with fluorophore-labeled Fab fragments for 5 min at room temperature. The Fab fragments/primary antibody molar ratio was 6:1. The mixture was followed by blocking solution for 5 min at the same ratio and applied to the slice for 5 h at room temperature. Finally, the slices were washed four times in PBS with 0.1% Triton X-100 and mounted on glass slides with Permafluor (Beckman Coulter, Brea, CA, USA).

Each specimen was analyzed three-dimensionally with a $z$-axis interval of 0.84–0.87 μm under conventional confocal laser-scanning microscopy (LSM510META, Carl Zeiss) equipped with a 40× objective. All images were corrected for brightness and contrast using LSM Image Browser version 3.2 (Carl Zeiss), Photoshop version 6.0, (Adobe Systems Inc, San Jose, CA, USA) and ImageJ (http://rsbweb.nih.gov/ij/). The coexpression of phenotype markers was usually confirmed three-dimensionally under higher magnification.

### 2.4. Numerical and statistical analyses

The proliferation curves of newly generated cells were predicted for each type of lineage according to the following equation:

$$\text{Number of EGFP-expressing cells} = \prod_i (1 + f_i), \quad (1)$$

where $f_i$ is the frequency of cell division during the $i$th period after retrovirus inoculation. The following survival probability was calculated for each lineage and was summarized.

$$\text{Survival probability} = \frac{\text{Number of cells counted at 28 DPI}}{\text{Total number of cells produced during 1 - 28 DPI}}. \quad (2)$$

All data in the text are presented as mean ± SEM (number of observation), and statistical significance was assessed using the non-parametric tests as the distribution functions were mostly unpredictable.

## 3. Results

### 3.1. Phenotypes of newly generated cells in the slice culture

The gross appearances and cellular architecture of the cultured hippocampal slices were similar to those from living animals between 14 and 42 days *in vitro* (DIV) as noted in the previous studies (Stoppini et al., 1991; Okada et al., 1995; Kamada et al., 2004). Within several days post-inoculation (DPI), EGFP-expressing cells were recognized around SGZ of the suprapyramidal blade of the GCL as shown in Fig. 2A. Under daily surveillance of the injected sites by fluorescent microscopy, round EGFP-expressing cells appeared on 2–3 DPI (Fig. 2Bi). Some of them had proliferated (Fig. 2Bii and Bviii), and migrated. Occasionally, one of the newly generated cells was untraceable (Fig. 2Bvii and Bxi) whereas the other differentiated with neuron-like morphology (Fig. 2Bxii–xiv).

Phenotypes of the newly generated EGFP-expressing cells were investigated immunohistochemically at 17 DIV (3 DPI) using two antibodies, anti-nestin and anti-GFAP (Supplementary Fig. S1A). Among the EGFP-expressing cells in the GCL (21 slices, 117 cells), 20 cells (17%) were both nestin- and GFAP-positive ($Nestin^+/GFAP^+$), 24 cells (21%) were nestin-positive but GFAP-negative ($Nestin^+/GFAP^-$), 12 cells (10%) were nestin-negative but GFAP-positive ($Nestin^-/GFAP^+$), whereas 61 cells (52%) were positive for neither ($Nestin^-/GFAP^-$) (Supplementary Fig. S2A). In another series of experiments, the phenotypes of newly generated EGFP-expressing cells were identified by the combination of anti-nestin and anti-HuC/D (Supplementary Fig. S1B). Among the EGFP-expressing cells (21 slices, 113 cells), 39 cells (35%) were both nestin- and HuC/D-positive ($Nestin^+/Hu^+$), 19 cells (17%) were nestin-positive but HuC/D-negative ($Nestin^+/Hu^-$), 19 cells (17%) were nestin-negative but HuC/D-positive ($Nestin^-/Hu^+$), whereas 36 cells (32%) were positive for neither ($Nestin^-/Hu^-$) (Supplementary Fig. S2B).

After tracking the lineage of EGFP-expressing cells their final phenotypes were identified at 42 DIV (28 DPI) using two antibodies, anti-HuC/D and anti-GFAP (Fig. 3). Among 110 cells examined

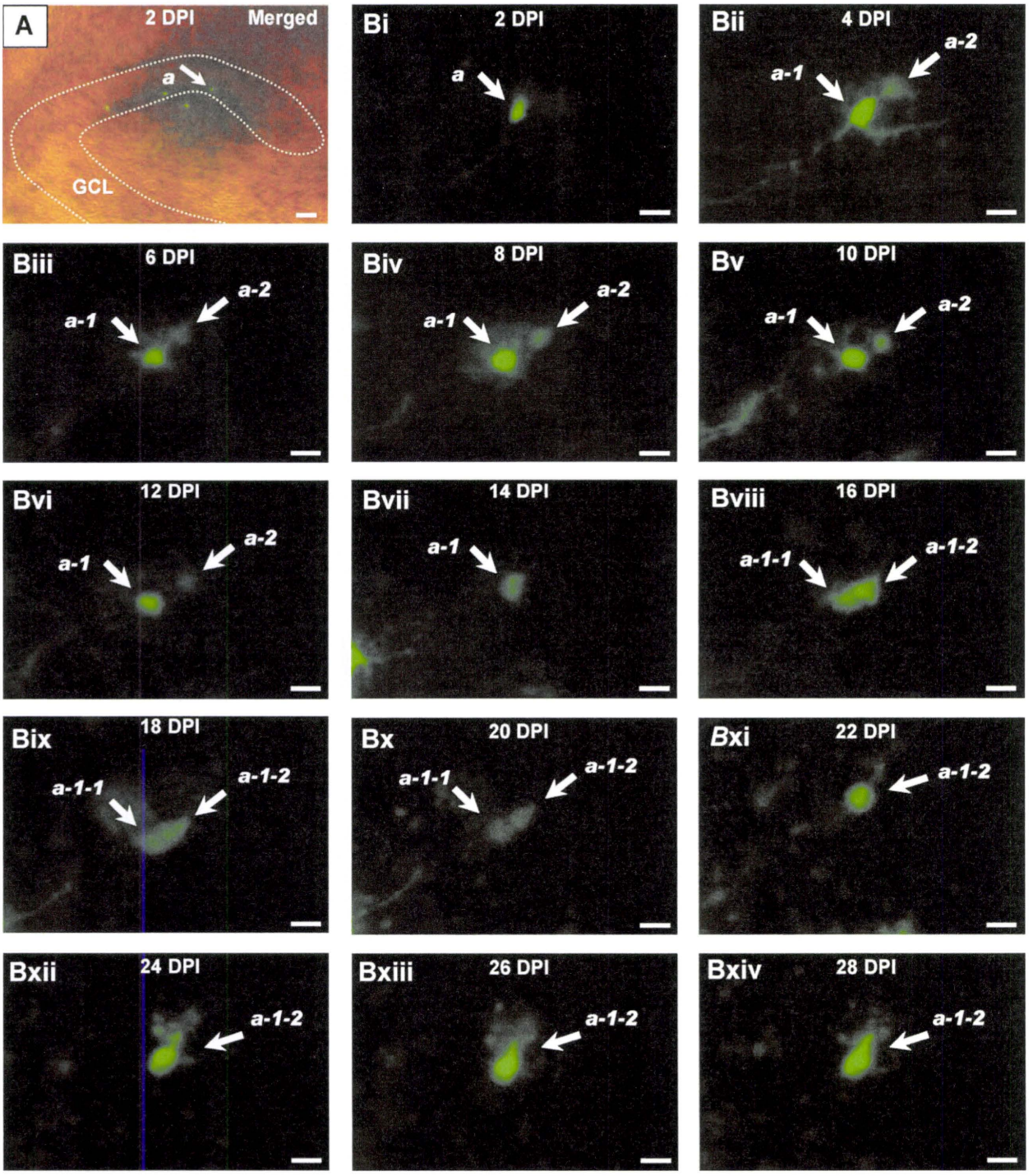


**Fig. 2.** Long-term survey of the newly generated cells in an organotypic culture of the hippocampus. (A) The slice culture at 2 DPI (16 DIV). The fluorescence image was overlaid on the plain picture. One of the EGFP-expressing cells (a, arrowed) was traced in Bi–ivx. GCL, the granule cell layer. (B) The daily surveillance of the fate of a newborn cell. A round EGFP-expressing cell, (a) was detected on the 2 DPI (Bi) and divided to produce a-1 and a-2 (Bii). One of them, a-2 became untraceable (Bvii) whereas another divided again to produce a-1-1 and a-1-2 (Bviii). One of them, a-1-1 became untraceable (Bxi), whereas another, a-1-2 differentiated with a neuronal morphology (Bxii–xiv). Scale bars, 100 μm in A and 20 μm in B.

(57 slices), 41 cells (37%) were HuC/D-positive but GFAP-negative ($Hu^+/GFAP^-$), 29 cells (26%) were GFAP-positive but HuC/D-negative ($Hu^-/GFAP^+$) and 40 cells (36%) were neither HuC/D- nor GFAP-positive ($Hu^-/GFAP^-$). We could not find any cells that were both HuC/D- and GFAP-positive. Therefore, according to the triple fluorescent labeling (anti-EGFP, anti-HuC/D and anti-GFAP), we classified the lineage of an EGFP-expressing cell as either "HuC/D-positive" or "GFAP-positive" groups. The cells that were negative to both HuC/D and GFAP were grouped as "unclassified". Some of the EGFP-expressing cells, which had dendrite-like processes (Fig. 3Ai), showed coexpression of HuC/D (Fig. 3Aii and B) but not GFAP (Fig. 3Aiii and Aiv). Other EGFP-positive cells with star-like appearances (Fig. 3Ci) were HuC/D-negative (Fig. 3Cii) and GFAP-positive (Fig. 3Ciii and Civ). We also found EGFP-positive, HuC/D-negative and GFAP-positive cells with the appearance of radial glia (Fig. 3Di–iv).

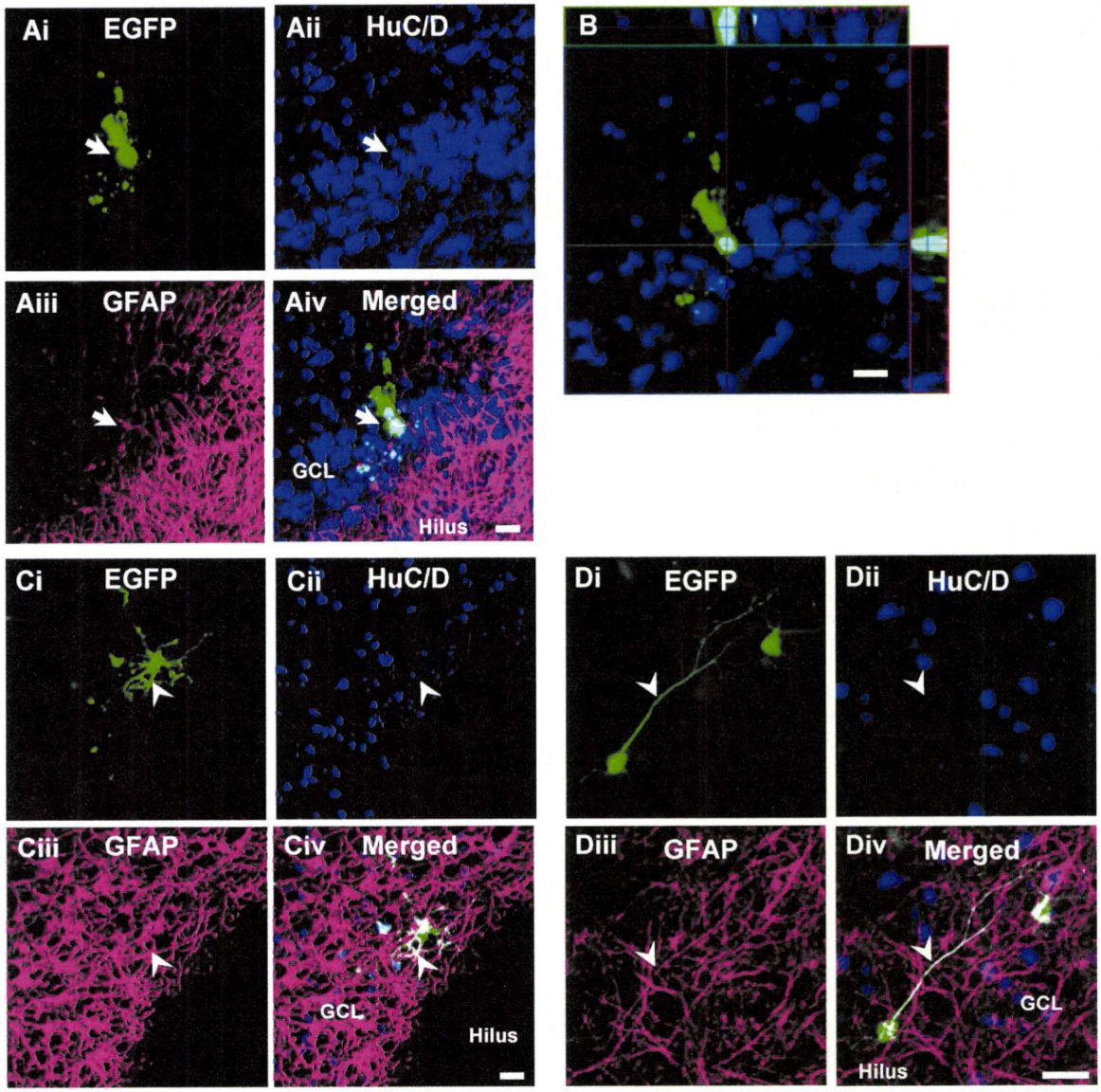


**Fig. 3.** Phenotype determination of the lineages. (A) A HuC/D-positive lineage cell. The phenotype of one of the EGFP-expressing cells (Ai, arrow) was examined immunohistochemically by using either anti-HuC/D antibody (Aii) or anti-GFAP antibody (Aiii). The merged image indicates that this cell is positive for HuC/D but negative for GFAP (Aiv). (B) Three-dimensional analysis of the cell shown in (A). (C) Similar to Ai–iv but the GFAP-positive lineage cell with an astrocyte-like appearance. (D) Another GFAP-positive lineage cell with a radial glia-like appearance. Scale bars, 20 μm.

Among all 87 lineages examined, 30 lineages (34%) were HuC/D-positive (Supplementary Fig. S3) and 15 lineages (17%) were GFAP-positive (Supplementary Fig. S4). When one of the descendent cells was HuC/D-positive, no GFAP-positive cells were generated in the same lineage as we examined. However, pair of "unclassified" cells was generated in one lineage. When one of the descendent cells was GFAP-positive, other members in the same lineage were also GFAP-positive. Again, no HuC/D-positive cells were found in any GFAP-positive lineage as we examined. The remaining lineages were unclassified as all the descendents became untraceable before 28 DPI ($n = 21$, 24%), or they were neither HuC/D- nor GFAP-positive ($n = 21$, 25%) (Supplementary Fig. S5). These lineages were not included in the following numerical analyses.

### 3.2. Quantitative analysis of the lineages

Among the HuC/D-positive lineages, 10/30 lineages showed no further proliferation, 10/30 divided once after EGFP expression and 10/30 divided more than twice. The EGFP-expressing cells were occasionally detectable as pairs opposite to each other (dividing pairs) (Kamada et al., 2004). As a result, 63 cells were finally produced. However, 23/63 cells were untraceable shortly after division in the searching field whereas others were traceable as long as up to 28 DPI. On the other hand, in the GFAP-positive lineage, the newly generated cells were rarely untraceable.

The frequency of cell division was summarized for both the HuC/D-positive (Fig. 4A) and the GFAP-positive groups (Fig. 4B) in each 1–7, 8–14, 15–21 or 22–28 DPI period. In both groups of lineages, the frequency was higher during the early DPI period (1–7 and 7–14) than the later (15–21 and 22–28 DPI) with significant differences ($P < 0.05$, One-way ANOVA with post hoc Scheffe's $F$-test). As shown in Fig. 4C, the proliferation of HuC/D-positive lineage cells was significantly less than expected from the predicted value ($P < 0.05$, One-sample Wilcoxon signed rank test). This is in contrast to that of GFAP-positive lineage cells, which was almost identical to the prediction (Fig. 4D). This difference could be attributed to the presence of large numbers of untraceable cells after cell division in the HuC/D-positive lineages. As summarized in Fig. 4E, the survival probability was $0.73 \pm 0.05$ ($n = 30$) in the HuC/D-positive lineages,

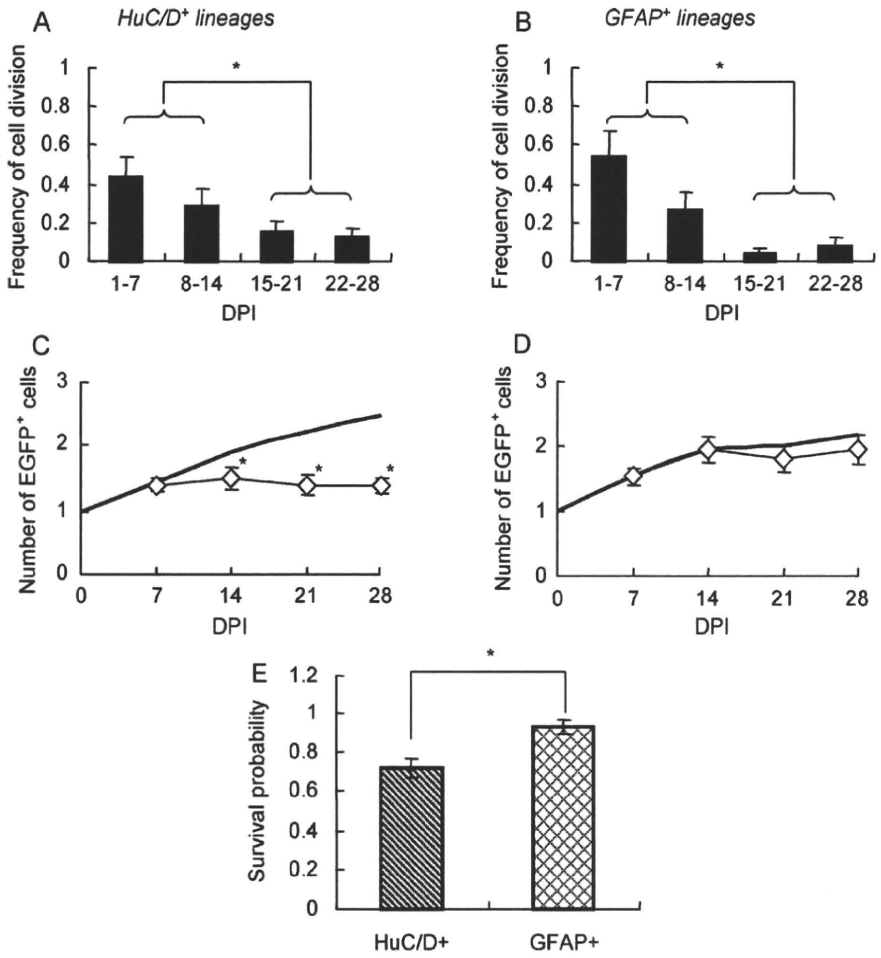


**Fig. 4.** Proliferation of newborn cells. A and C from the HuC/D-positive lineages ($n = 30$) and B and D from the GFAP-positive lineages ($n = 15$). (A, B) The frequency of cell division during each of the four period 1–7, 8–14, 15–21 and 22–28 DPI (mean ± SEM). The difference was statistically examined (One-way ANOVA with post hoc Scheffe's *F*-test) between the early DPI period (1–7 and 7–14) and the later (15–21 and 22–28 DPI). *$P < 0.05$. (C, D) The time-dependent change of the number of EGFP-expressing cells (open symbols and bars, mean ± SEM). The thick line is the proliferation curve expected from the frequency of cell division shown in A or B. * indicates the significant difference from the prediction ($P < 0.05$, One-sample Wilcoxon signed rank test). (E) Summary of the survival probability (mean ± SEM) in the HuC/D-positive and GFAP-positive lineages. *$P < 0.01$ (Mann–Whitney *U*-test).

which was significantly smaller than that in the GFAP-positive lineages (0.93 ± 0.05, $n = 15$; $P < 0.05$, Mann–Whitney *U*-test).

In 18/30 HuC/D-positive lineages one of the newly divided cells survived as long as 28 DPI, whereas another became untraceable. The follow-up period was distributed between 7 and 25 days with a mean of 17.9 ± 1.1 DPI ($n = 25$) (Fig. 5A). However, 11/25 cells became untraceable after the second division, 9/25 cells after the third division and 1/25 cells after the fourth division. Therefore, the postmitotic period of an untraceable cell was measured directly from the lineage tree and was summarized in Fig. 5B. It distributed between 2 and 14 days (mean, 6.5 ± 0.8 days; $n = 25$). The postmitotic period was also measured for 21 lineages in which all the descendents became untraceable before 28 DPI. Similar to that of the HuC/D-positive lineages, its distribution was between 1 and 16 days (mean, 7.7 ± 0.7 days; $n = 31$, Supplementary Fig. S6C).

### 3.3. Differentiation of neuron-like descendents

We also identified the phenotypes of EGFP-expressing cells immunohistochemically at 28 DPI by other markers, Prox1 and NeuN. As shown in Fig. 6Ai–iv and B, some of the Prox1- and EGFP-expressing cells were also positive for NeuN, and designated as Prox1$^+$/NeuN$^+$ cells. On the other hand, a significant number of the Prox1-positive cells did not express NeuN (Prox1$^+$/NeuN$^-$ cells) (Fig. 6Ci–iv, D). A small number of the EGFP-expressing cells (2 in 71 cells examined) were positive for NeuN, but negative for Prox1 (Prox1$^-$/NeuN$^+$). Among 49 lineages producing Prox1-positive cells (Supplementary Fig. S7), both NeuN-positive and NeuN-negative cells arose in 3/49 lineage. Among 23 cases of the last division in the Prox1$^+$/NeuN$^+$ lineages, 8 cases had two Prox1$^+$/NeuN$^+$ cells, 9 cases had one untraceable cell and 3 cases had two untraceable cells. In another 3 cases, one of the descendents was NeuN-negative. In both Prox1$^+$/NeuN$^-$ (Fig. 7A) and Prox1$^+$/NeuN$^+$ (Fig. 7B) lineages, the frequency of cell division was higher during the early DPI period (1–7 and 7–14) than the later (15–21 and 22–28 DPI) with significant differences ($P < 0.05$, One-way ANOVA with post hoc Scheffe's *F*-test). Newly divided cells became often untraceable in either lineage of Prox1$^+$/NeuN$^+$ or Prox1$^+$/NeuN$^-$ cells. Among 71 cells that were finally produced, 28/71 became untraceable shortly after division in the searching field whereas others were traceable as long as up to 28 DPI. Once untraceable, they never reappeared at 28 DPI under confocal microscopy with anti-EGFP immunohistochemistry even when they became untraceable only a few days before. As a result, the proliferation was significantly less than expected from the predicted value at 28 DPI in the Prox1$^+$/NeuN$^-$ lineage group (Fig. 7C) ($P < 0.05$, One-sample Wilcoxon signed rank test) and was significantly less than expected at 14, 21 and 28 DPI in the Prox1$^+$/NeuN$^+$ lineage group (Fig. 7D) ($P < 0.05$, One-sample Wilcoxon signed rank test). The postmitotic period of an untraceable cell distributed between 2 and 18 days (mean, 6.3 ± 1.5

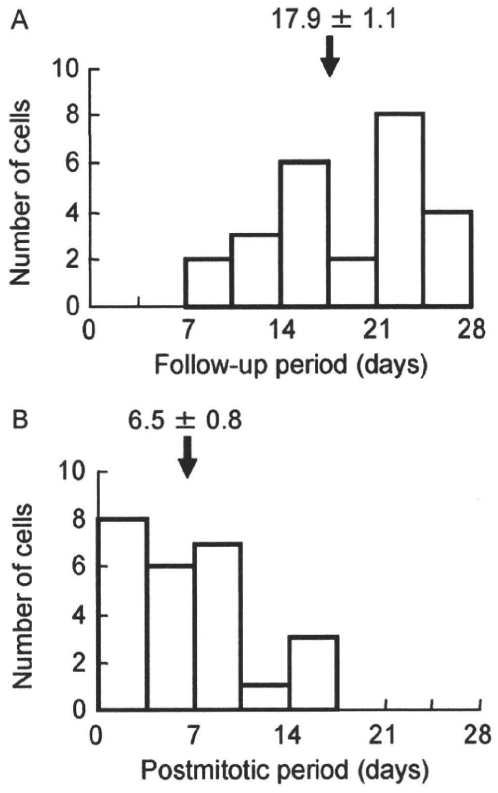


**Fig. 5.** Lifetime analysis. (A) Histogram of the follow-up periods in the HuC/D-positive lineages ($n = 25$). (B) Histogram of the postmitotic periods of untraceable cells ($n = 25$). Arrows and numbers indicate the mean (±SEM) values.

days; $n = 11$) for the Prox1$^+$/NeuN$^-$ lineages (Fig. 7E), whereas it did between 2 and 10 days (mean, 5.3 ± 0.5 days; $n = 22$) for the Prox1$^+$/NeuN$^+$ lineages (Fig. 7F). There was no significant difference in the postmitotic period ($P > 0.9$, Kolmogorov–Smirnov test). The postmitotic period was measured also for the phenotypically identified GCL neuron. It was distributed between 3 and 26 days (mean, 15.0 ± 2.0 days; $n = 44$) for the Prox1$^+$/NeuN$^-$ lineages (Fig. 7G) with insignificant difference from that of untraceable cells ($P > 0.05$, Kolmogorov–Smirnov test). However, 12/25 cells survived over 23 days. For the Prox1$^+$/NeuN$^+$ lineages, as shown in Fig. 7H, it was between 12 and 28 days (mean, 20.1 ± 0.6 days; $n = 44$) with negligible overlap of the postmitotic period distribution of the untraceable cells ($P < 10^{-12}$, Kolmogorov–Smirnov test).

## 4. Discussion

In the present study, we identified newly generated cells using a retroviral labeling method in an organotypic slice culture of the hippocampus. This method enabled us to survey the lineage of a newborn cell up to 28 DPI and to determine retrospectively the phenotype of the descendent cells using the specific markers, HuC/D, GFAP, Prox1 and NeuN. In our experiments, slices were usually obtained from the dorsal part of rat hippocampus at P7, the retroviruses were inoculated restrictively in the suprapyramidal blade of GCL at 14 DIV and the fate of the EGFP-expressing cells were followed up only in the suprapyramidal region. Although it is possible that the region- or age-dependent difference of neurogenic ability is present, we did not do any systematic study on it.

### 4.1. The phenotypes of newly generated EGFP-expressing cells

When we identified the phenotypes of the newly generated cells at 3 DPI, we found in the GCL that 17% were positive for both nestin and GFAP and that 35% were positive for both nestin and HuC/D. Therefore, these newly divided cells consisted of both multi-potent type-1 cells which express both nestin and GFAP (Kempermann et al., 2004; Steiner et al., 2006; Roybon et al., 2009) and the neuron-destined type-2, -3 cells which express both nestin and HuC/D (Steiner et al., 2004; Seki et al., 2007). Nestin-negative and HuC/D-positive cells (17%) and a subpopulation of cells which were neither positive to nestin nor GFAP (52%) can be classified into newborn neurons. However, there remains the EGFP-expressing cells neither nestin nor HuC/D (32%) and those negative to nestin, HuC/D and GFAP (estimated to be 35%). Some of them are possibly involved in non-neuronal lineages such as proliferating astrocytes, oligodendrocytes and microglia. The pluripotent NG2 cells are possibly included in these cells (Belachew et al., 2003; Thallmair et al., 2006; Rivers et al., 2008; Zhu et al., 2008). In our slice culture, GCL neurons are clustering in the relatively thin layer under the astrocytic layer (Kamada et al., 2004). It is possible that some of these covering astrocytes are proliferating in the slice culture (Namba et al., 2005). Although the neuronal network became stabilized before 14 DIV (Buchs et al., 1993) after transient rearrangements (Robain et al., 1994; Gutierrez and Heinemann, 1999) in the slice culture, the proliferating cells may be populationally different from those in the adult animals. These possibilities have to be tested in the future by using markers specific to each cell type.

### 4.2. Neuron-generating lineages

In the present study, no evidence was found that the GFAP-positive cells arose in the HuC/D-positive lineage. Rather, when one of the descendants was HuC/D-positive, most of the other cells in the same lineage were also HuC/D-positive. In some lineages HuC/D-positive cells were generated after several cell divisions. Similarly, when one of the descendants was Prox1- or NeuN-positive, other cells in the same lineage were mostly Prox1- or NeuN-positive. These results suggest the presence of neuron-generating lineages which are destined to produce neurons, although we have no evidence if they are derived from the multipotent type-1 cells or the transiently amplifying type-2, -3 cells.

In the groups of HuC/D-positive lineages, the frequency of cell division was higher in the early DPI period (1–14 DPI) than in the late (15–28 DPI). Almost similar results were observed for the Prox1- or NeuN-positive lineage group. That is, many of the differentiated cells were produced early DPI period in the neuron-generating lineage. We could not find the exact reasons, but it is possible that we are preferentially tracked the cells that are in the later proliferative phase such as the transiently amplifying type-2, -3 cells. This is also the case for our GFAP-positive lineage group. On the other hand, the frequency of cell division was almost even throughout the tracking period in the HuC/D-negative lineage subgroup of unclassified group (Supplementary Fig. S6A). It is possible that the highly proliferative cells were included in this subgroup. The proliferation of HuC/D-negative lineage cells was no less than expected from the prediction (Supplementary Fig. S6B) as the newly divided cells became rarely untraceable.

### 4.3. Critical traceablility period

While the neuron-generating lineages produced HuC/D-, Prox1- or NeuN-positive descendants, other descendents became frequently untraceable. Once untraceable, these cells never reappeared even under close inspection after immunohistochemistry using anti-EGFP antibody. We also found a significant number of the unclassified lineages in which all the descendents were untraceable before phenotype identification (Supplementary Fig. S5). This is in contrast to the GFAP-positive lineages in which most

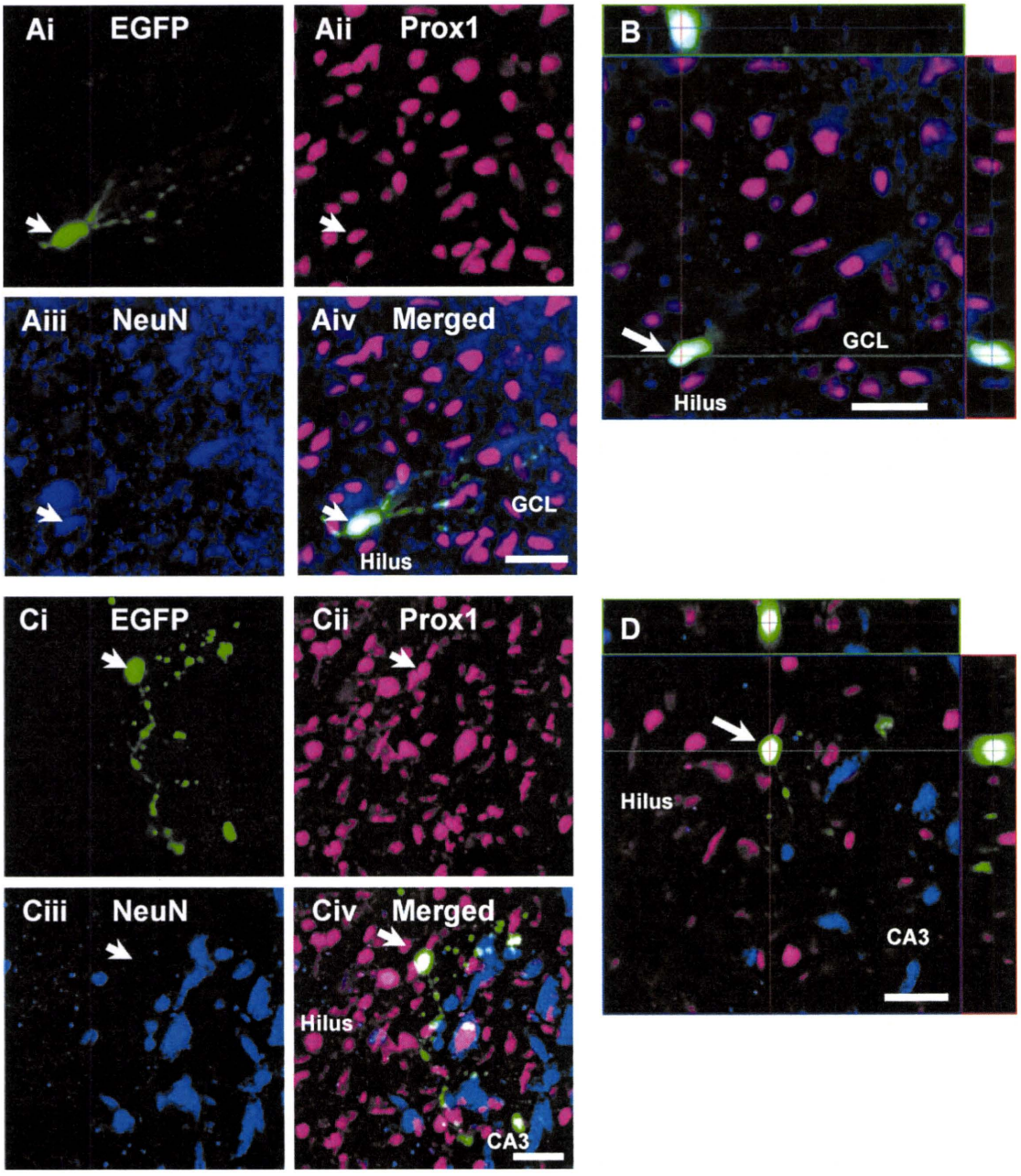


**Fig. 6.** Immunohistochemical study of differentiation. (A) A mature dentate granule cell layer (GCL) neuron. The phenotype of one of the EGFP-expressing cells (Ai, arrow) was examined immunohistochemically by using either anti-Prox1 antibody (Aii) or anti-NeuN antibody (Aiii). The merged image indicates that this cell is Prox1$^+$/NeuN$^+$ (Aiv) and judged as a mature GCL neuron. (B) Three-dimensional analysis of the cell shown in (Ai–iv). (C) A immature GCL neuron (arrow) that is positive for Prox1 but negative for NeuN, indicated as Prox1$^+$/NeuN$^-$. (D) Three-dimensional analysis of the cell shown in (Ci–iv). Scale bars, 20 μm.

of the descendants were traceable up to 28 DPI. The above postmitotic untraceability is consistent with the previous *in vivo* studies describing that substantial numbers (30–70%) of newly generated cells undergo cell death (Cameron and McKay, 2001; Dayer et al., 2003; Sun et al., 2004). Programmed cell death during normal development has been reported to occur ubiquitously throughout the central and peripheral nervous system of vertebrates and invertebrates (Purves and Lichtman, 1985; Jacobson, 1993; Buss et al., 2006). A quantitative matching of neurons with their targets and afferents is thereby attained. Analogous to the programmed cell death during embryonic period, some of the newly generated neurons might become untraceable as a result of apoptosis (Gould and McEwen, 1993; Krantic et al., 2007) although further study is necessary. It remains possible that some of the cells became untraceable due to other reasons such as migration out of the inspecting fields. However, the incidence of cell untraceability was high during the early postmitotic phase, suggesting the presence of a certain critical period. We refer it as "critical traceability period" to differentiate from the critical period of cell death.

In the postnatal hippocampus, the numbers of newly generated neurons were reduced at a high rate between 6 and 28 days after they were labeled with 5-bromodeoxyuridine (BrdU) but were stable between 1 and 6 months (Dayer et al., 2003; Kempermann et al., 2003). New neurons that expressed GFP by the retrovirus method reduced in density within 3 weeks of virus injection (Tashiro et al., 2006). However, hitherto little has been known about the actual lifespan of newly generated neurons. In the organotypic slice culture of hippocampus the EGFP-labeled new neurons could be tracked as lineages. The critical traceability period was thus measured for individual cells and was 2–14 days after their last division

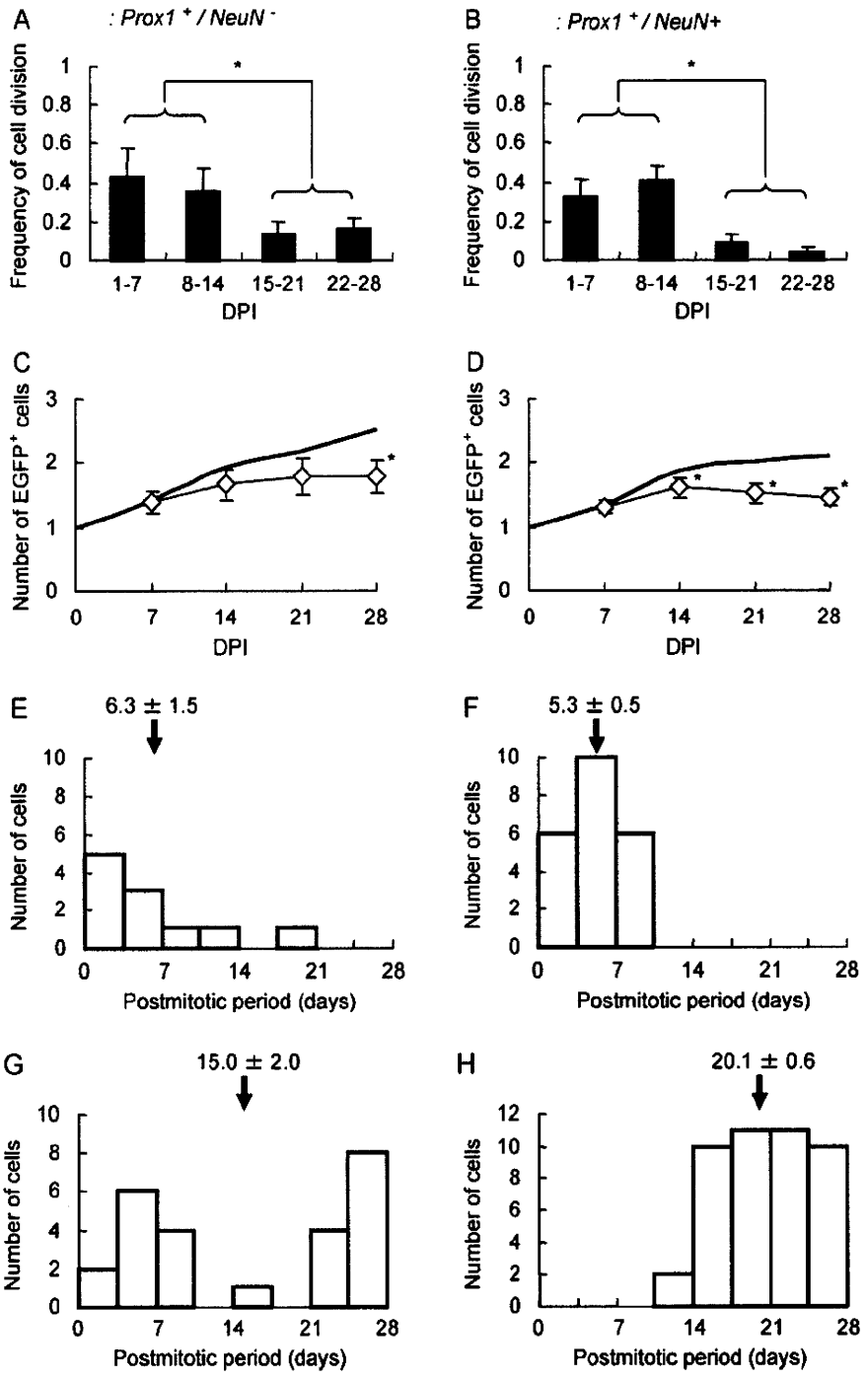


**Fig. 7.** Analysis of the differentiating lineages. A, C, E and G from the Prox1$^+$/NeuN$^-$ lineages ($n$ = 18) and B, D, F and H from the Prox1$^+$/NeuN$^+$ lineages ($n$ = 34). Note that three lineages were overlapped. (A, B) The frequency of cell division during each of the four period 1–7, 8–14, 15–21 and 22–28 DPI (mean ± SEM). The difference was statistically examined (One-way ANOVA with post hoc Scheffe's $F$-test) between the early DPI period (1–7 and 7–14) and the later (15–21 and 22–28 DPI). *$P$ < 0.05. (C, D) The time-dependent change of the number of EGFP-expressing cells (open symbols and bars, mean ± SEM). The thick line is the proliferation curve expected from the frequency of cell division (A or B). * indicates the significant difference from the prediction ($P$ < 0.05, One-sample Wilcoxon signed rank test). (E, F) Histograms of the postmitotic periods. Arrows and numbers indicate the mean (±SEM) values. (G, H) Histograms of the postmitotic periods of the immature and mature GCL neurons, respectively. Arrows and numbers indicate the mean (±SEM) values.

in the HuC/D-positive lineages. A similar critical traceability period was observed in both the Prox1$^+$/NeuN$^-$ lineages that generated immature GCL neurons (2–18 days) and the Prox1$^+$/NeuN$^+$ lineages that generated mature GCL neurons (2–10 days). Therefore, it is suggested that a neuron differentiates into its mature form once it survives this period. Consistent with this notion, none of the differentiated GCL neurons that expressed both Prox1 and NeuN had a postmitotic period of less than 12 days. It is possible that a newborn neuron differentiates into its mature form through some key processes that determine its fate.

## 5. Conclusions

The present experimental system enabled us to track a single progenitor cell and its descendents as a lineage using the organotypic culture of hippocampus as an *ex vivo* model of the post-

natal hippocampus. The lineage was identified retrospectively as neuron-generating using an immunohistochemical marker, HuC/D. We found that (1) the descendent cells of the neuron-generating lineages were mostly GFAP-negative, (2) the newly generated cells became frequently untraceable in the neuron-generating lineages and (3) this critical traceability period was 2–14 days. It is suggested that newly generated neurons differentiate into mature GCL neurons once they survive this period. The adult neurogenesis is under the influence of the local network activity and/or the SGZ niche in the *in vivo* hippocampus (Lie et al., 2005; Ge et al., 2006; Tashiro et al., 2006; Kuwabara et al., 2009). Our lineage analysis methods using slice culture system would be advantageous to test several hypotheses concerning these regulatory mechanisms under experimental manipulations.

## Acknowledgements

We thank Y. Sugiyama for technical advice and D.B.L. Teh and B. Bell for language assistance.

## Appendix A. Supplementary data

Supplementary data associated with this article can be found, in the online version, at doi:10.1016/j.neures.2010.11.010.

## References

Aimone, J.B., Willes, J., Gage, F.H., 2006. Potential role for adult neurogenesis in the encoding of time in new memories. Nat. Neurosci. 9, 723–727.
Akamatsu, W., Fujihara, H., Mitsuhashi, T., Yano, M., Shibata, S., Hayakawa, Y., Okano, J.H., Sakakibara, S., Takano, H., Takano, T., Takahashi, T., Noda, T., Okano, H., 2005. The RNA-binding protein HuD regulates neuronal cell identity and maturation. Proc. Natl. Acad. Sci. U.S.A. 22, 4625–4630.
Alfonoso, L., Guillermo, O., 2007. Prox1 expression patterns in the developing and adult murine brain. Dev. Dyn. 236, 518–524.
Altman, J., Das, G.D., 1965. Autoradiographic and histological evidence of postnatal hippocampal neurogenesis in rats. J. Comp. Neurol. 124, 319–336.
Belachew, S., Chittajallu, R., Aguirre, A.A., Yuan, X., Kirby, M., Anderson, S., Gallo, V., 2003. Postnatal NG2 proteoglycan-expressing progenitor cells are intrinsically multipotent and generate functional neurons. J. Cell Biol. 161, 169–186.
Brown, J.P., Couillard-Després, S., Cooper-Kuhn, C.M., Winkler, J., Aigner, L., Kuhn, H.G., 2003. Transient expression of doublecortin during adult neurogenesis. J. Comp. Neurol. 467, 1–10.
Bruel-Jungerman, E., Laroche, S., Rampon, C., 2005. New neurons in the dentate gyrus are involved in the expression of enhanced long-term memory following environmental enrichment. Eur. J. Neurosci. 21, 513–521.
Bruel-Jungerman, E., Davis, S., Rampon, C., Laroche, S., 2006. Long-term potentiation enhances neurogenesis in the adult dentate gyrus. J. Neurosci. 26, 5888–5893.
Buchs, P.A., Stoppini, L., Muller, D., 1993. Structural modifications associated with synaptic development in area CA1 of rat hippocampal organotypic cultures. Dev. Brain Res. 71, 81–91.
Buss, R.R., Sun, W., Oppenheim, R.W., 2006. Adaptive roles of programmed cell death during nervous system development. Annu. Rev. Neurosci. 29, 1–35.
Cameron, H.A., Woolley, C.S., McEwen, B.S., Gould, E., 1993. Differentiation of newly born neurons and glia in the dentate gyrus of the adult rat. Neuroscience 56, 337–344.
Cameron, H.A., McKay, R.D., 2001. Adult neurogenesis produces a large pool of new granule cells in the dentate gyrus. J. Comp. Neurol. 435, 406–412.
Dailey, M.E., Buchanan, J., Bergles, D.E., Smith, S.J., 1994. Mossy fiber growth and synaptogenesis in rat hippocampal slices in vitro. J. Neurosci. 14, 1060–1078.
Dayer, A.G., Ford, A.A., Cleaver, K.M., Yassaee, M., Cameron, H.A., 2003. Short-term and long-term survival of new neurons in the rat dentate gyrus. J. Comp. Neurol. 460, 563–572.
Dupret, D., Revest, J.M., Koehl, M., Ichas, F., De Giorgi, F., Costet, P., Abrous, D.N., Piazza, P.V., 2008. Spatial relational memory requires hippocampal adult neurogenesis. PLoS ONE 3 (4), e1959, doi:10.1371/journal.pone.0001959.
Eriksson, P.S., Perfilieva, E., Björk-Eriksson, T., Alborn, A.M., Nordborg, C., Peterson, D.A., Gage, F.H., 1998. Neurogenesis in the adult human hippocampus. Nat. Med. 4, 1313–1317.
Ernst, C., Christie, B.R., 2005. The putative neural stem cell marker, nestin, is expressed in heterogeneous cell types in the adult rat neocortex. Neuroscience 138, 183–188.
Filippov, V., Kronenberg, G., Pivneva, T., Reuter, K., Steiner, B., Wang, L.P., Yamaguchi, M., Kettenmann, H., Kempermann, G., 2003. Subpopulation of nestin-expressing progenitor cells in the adult murine hippocampus shows electrophysiological and morphological characteristics of astrocytes. Mol. Cell. Neurosci. 23, 373–382.
Fukuda, S., Kato, F., Tozuka, Y., Yamaguchi, M., Miyamoto, Y., Hisatsune, T., 2003. Two distinct subpopulations of nestin-positive cells in adult mouse dentate gyrus. J. Neurosci. 23, 9357–9366.
Galeeva, A., Treuter, E., Tomarev, S., Pelto-Huikko, M., 2007. A prospero-related homeobox gene Prox-1 is expressed during postnatal brain development as well as in the adult rodent brain. Neuroscience 146, 604–616.
Gähwiler, B.H., 1984. Development of the hippocampus in vitro: cell types, synapses and receptors. Neuroscience 11, 751–760.
Gähwiler, B.H., Capogna, M., Debanne, D., McKinney, R.A., Thompson, S.M., 1997. Organotypic slice cultures: a technique has come of age. Trends Neurosci. 20, 471–477.
Ge, S., Goh, E.L.K., Sailor, K.A., Kitabatake, Y., Ming, G.L., Song, H., 2006. GABA regulates synaptic integration of newly generated neurons in the adult brain. Nature 439, 589–593.
Goldman, S., 2003. Glia as neural progenitor cells. Trends Neurosci. 26, 590–596.
Gould, E., McEwen, B.S., 1993. Neuronal birth and death. Curr. Opin. Neurobiol. 3, 676–682.
Gutierrez, R., Heinemann, U., 1999. Synaptic reorganization in explanted cultures of rat hippocampus. Brain Res. 815, 304–316.
Imayoshi, I., Sakamoto, M., Ohtsuka, T., Takao, K., Miyakawa, T., Yamaguchi, M., Mori, K., Ikeda, T., Itohara, S., Kageyama, R., 2008. Role of continuous neurogenesis in the structural and functional integrity of the adult forebrain. Nat. Neurosci. 11, 1153–1161.
Jacobson, M., 1993. Developmental Neurobiology, third ed. Plenum Press, New York, NY.
Kamada, M., Li, R.Y., Hashimoto, M., Kakuda, M., Okada, H., Koyanagi, Y., Ishizuka, T., Yawo, H., 2004. Intrinsic and spontaneous neurogenesis in the postnatal slice culture of rat hippocampus. Eur. J. Neurosci. 20, 2499–2508.
Kempermann, G., Kuhn, H.G., Gage, F.H., 1997. More hippocampal neurons in adult mice living in an enriched environment. Nature 386, 493–495.
Kempermann, G., Gast, D., Kronenberg, G., Yamaguchi, M., Gage, F.H., 2003. Early determination and long-term persistence of adult-generated new neurons in the hippocampus of mice. Development 130, 391–399.
Kempermann, G., Jessberger, S., Steiner, B., Kronenberg, G., 2004. Milestones of neuronal development in the adult hippocampus. Trends Neurosci. 27, 447–452.
Kempermann, G., 2008. The neurogenic reserve hypothesis: what is adult neurogenesis good for? Trends Neurosci. 31, 163–169.
Krantic, S., Mechawar, N., Reix, S., Quirion, R., 2007. Apoptosis-inducing factor: a matter of neuron life and death. Prog. Neurobiol. 81, 179–196.
Kronenberg, G., Reuter, K., Steiner, B., Brandt, M.D., Jessberger, S., Yamagushi, M., Kempermann, G., 2003. Subpopulations of proliferating cells of the adult hippocampus respond differently to physiologic neurogenic stimuli. J. Comp. Neurol. 467, 455–463.
Kuwabara, T., Hsieh, J., Muotri, A., Yeo, G., Warashina, M., Lie, D.C., Moore, L., Nakashima, K., 2009. Wnt-mediated activation of NeuroD1 and retro-elements during adult neurogenesis. Nat. Neurosci. 12, 1097–1105.
Lagace, D.C., Whitman, M.C., Noonan, M.A., Ables, J.L., DeCarolis, N.A., Arguello, A.A., Donovan, M.H., Fischer, S.J., Farnbauch, L.A., Beech, R.D., DiLeone, R.J., Greer, C.A., Mandyam, C.D., Eisch, A.J., 2007. Dynamic contribution of nestin-expressing stem cells to adult neurogenesis. J. Neurosci. 27, 12623–12629.
Laskowski, A., Schmidt, W., Dinkel, K., Martínez-Sánchez, M., Reymann, K.G., 2005. bFGF and EGF modulate trauma-induced proliferation and neurogenesis in juvenile organotypic hippocampal slice cultures. Brain Res. 1037, 78–89.
Lendahl, U., Zimmerman, L.B., McKay, R.D., 1990. CNS stem cells express a new class of intermediate filament protein. Cell 60, 585–595.
Lie, D.C., Colamarino, S.A., Song, H.J., Désiré, L., Mira, H., Consiglio, A., Lein, E.S., Jessberger, S., Lansford, H., Dearie, A.R., Gage, F.H., 2005. Wnt signalling regulates adult hippocampal neurogenesis. Nature 437, 1370–1375.
Lledo, P.M., Alonso, M., Grubb, M.S., 2006. Adult neurogenesis and functional plasticity in neuronal circuits. Nat. Rev. Neurosci. 7, 179–193.
Meshi, D., Drew, M.R., Saxe, M., Ansorge, M.S., David, D., Santarelli, L., Malapani, C., Moore, H., Hen, R., 2006. Hippocampal neurogenesis is not required for behavioral effects of environmental enrichment. Nat. Neurosci. 9, 729–731.
Namba, T., Mochizuki, H., Onodera, M., Mizuno, Y., Namiki, H., Seki, T., 2005. The fate of neural progenitor cells expressing astrocytic and radial glial markers in the postnatal rat dentate gyrus. Eur. J. Neurosci. 22, 1928–1941.
Namba, T., Mochizuki, H., Onodera, M., Namiki, H., Seki, T., 2007. Postnatal neurogenesis in hippocampal slice cultures: early in vitro labeling of neural precursor cells leads to efficient neuronal production. J. Neurosci. Res. 85, 1704–1712.
Okada, M., Sakaguchi, T., Kawasaki, K., 1995. Correlation between anti-ubiquitin immunoreactivity and region-specific neuronal death in N-methyl-D-aspartate-treated rat hippocampal organotypic cultures. Neurosci. Res. 22, 359–366.
Palmer, T.D., Takahashi, J., Gage, F.H., 1997. The adult rat hippocampus contains primordial neural stem cells. Mol. Cell. Neurosci. 8, 389–404.
Poulsen, F.R., Blaabjerg, M., Montero, M., Zimmer, J., 2005. Glutamate receptor antagonists and growth factors modulate dentate granule cell neurogenesis in organotypic, rat hippocampal slice cultures. Brain Res. 1051, 35–49.
Purves, D., Lichtman, J.W., 1985. Principles of Neural Development. Sinauer Associates, Inc., Sunderland, MA.
Raineteau, O., Rietschin, L., Gradwohl, G., Guillemot, F., Gähwiler, B.H., 2004. Neurogenesis in hippocampal slice cultures. Mol. Cell. Neurosci. 26, 241–250.
Rivers, L.E., Young, K.M., Rizzi, M., Jamen, F., Psachoulia, K., Wada, A., Kessaris, N., Richardson, W.D., 2008. PDGFRA/NG2 glia generate myelinating oligodendrocytes and piriform projection neurons in adult mice. Nat. Neurosci. 11, 1392–1401.

Robain, O., Barbin, G., Billette de Villemeur, T., Jardin, L., Jahchan, T., Ben-Ari, Y., 1994. Development of mossy fiber synapses in hippocampal slice culture. Dev. Brain Res. 80, 244–250.
Roybon, L., Hjalt, T., Stott, S., Guillemot, F., Li, J.Y., Brundin, P., 2009. Neurogenin2 directs granule neuroblast production and amplification while NeuroD1 specifies neuronal fate during hippocampal neurogenesis. PLoS ONE 4 (3), e4779, doi:10.1371/journal.pone.0004779.
Sakaguchi, T., Okada, M., Kawasaki, K., 1994. Sprouting of CA3 pyramidal neurons to the dentate gyrus in rat hippocampal organotypic cultures. Neurosci. Res. 20, 157–164.
Saxe, M.D., Battaglia, F., Wang, J.W., Malleret, G., David, D.J., Monckton, J.E., Garcia, A.D., Sofroniew, M.V., Kandel, E.R., Santarelli, L., Hen, R., Drew, M.R., 2006. Ablation of hippocampal neurogenesis impairs contextual fear conditioning and synaptic plasticity in the dentate gyrus. Proc. Natl. Acad. Sci. U.S.A. 103, 17501–17506.
Seki, T., Namba, T., Mochizuki, H., Onodera, M., 2007. Clustering, migration, and neurite formation of neural precursor cells in the adult rat hippocampus. J. Comp. Neurol. 502, 275–290.
Seri, B., García-Verdugo, J.M., McEwen, B.S., Alvarez-Buylla, A., 2001. Astrocytes give rise to new neurons in the adult mammalian hippocampus. J. Neurosci. 21, 7153–7160.
Seri, B., García-Verdugo, J.M., Collado-Morente, L., McEwen, B.S., Alvarez-Buylla, A., 2004. Cell types, lineage, and architecture of the germinal zone in the adult dentate gyrus. J. Comp. Neurol. 478, 359–378.
Steiner, B., Kronenberg, G., Jessberger, S., Brandt, M.D., Reuter, K., Kempermann, G., 2004. Differential regulation of gliogenesis in the context of adult hippocampal neurogenesis in mice. Glia 46, 41–52.
Steiner, B., Klempin, F., Wang, L.P., Kott, M., Kettenmann, H., Kempermann, G., 2006. Type-2 cells as link between glial and neuronal lineage in adult hippocampal neurogenesis. Glia 54, 805–814.
Steiner, B., Zurborg, S., Hrster, H., Fabel, K., Kempermann, G., 2008. Differential 24 h responsiveness of prox1-expressing precursor cells in adult hippocampal neurogenesis to physical activity, environmental enrichment, and kainic acid-induced seizures. Neuroscience 154, 521–529.
Stoppini, L., Buchs, P.A., Muller, D., 1991. A simple method for organotypic cultures of nervous tissue. J. Neurosci. Methods 37, 173–182.
Sun, W., Winseck, A., Vinsant, S., Park, O.H., Kim, H., Oppenheim, R.W., 2004. Programmed cell death of adult-generated hippocampal neurons is mediated by the proapoptotic gene Bax. J. Neurosci. 24, 11205–11213.
Tashiro, A., Sandler, V.M., Toni, N., Zhao, C., Gage, F.H., 2006. NMDA-receptor-mediated, cell-specific integration of new neurons in adult dentate gyrus. Nature 442, 929–933.
Thallmair, M., Ray, J., Stallcup, W.B., Gage, F.H., 2006. Functional and morphological effects of NG2 proteoglycan deletion on hippocampal neurogenesis. Exp. Neuro. 202, 167–178.
van Praag, H., Christie, B.R., Sejnowski, T.J., Gage, F.H., 1999. Running enhances neurogenesis, learning, and long-term potentiation in mice. Proc. Natl. Acad. Sci. U.S.A. 96, 13427-13431.72.
Wakamatsu, Y., Weston, J.A., 1997. Sequential expression and role of Hu RNA-binding proteins during neurogenesis. Development 124, 3449–3460.
Zhang, C.L., Zou, Y., He, W., Gage, F.H., Evans, R., 2008. A role for adult TLX-positive neural stem cells in learning and behaviour. Nature 451, 1004–1007.
Zhu, X., Bergles, D.E., Nishiyama, A., 2008. NG2 cells generate both oligodendrocytes and gray matter astrocytes. Development 135, 145–157.
Zimmer, J., Gähwiler, B.H., 1984. Cellular and connective organization of slice cultures of the rat hippocampus and fascia dentata. J. Comp. Neurol. 228, 432–446.

## Glossary

*BrdU:* 5-bromodeoxyuridine
*GCL:* granule cell layer
*EGFP:* enhanced green fluorescent protein
*GFAP:* glial fibrillary acidic protein
*NeuN:* neuronal nuclei antigen
*PBS:* phosphate-buffered saline
*Prox1:* prospero-related homeobox protein
*PSA-NCAM:* polysialyated neural cell adhesion molecule
*SGZ:* subgranular zone

OPEN ACCESS Freely available online

PLoS one

# Opto-Current-Clamp Actuation of Cortical Neurons Using a Strategically Designed Channelrhodopsin

**Lei Wen[1,2,3◔], Hongxia Wang[1,2,3◔], Saki Tanimoto[1,2,3], Ryo Egawa[1,2,3], Yoshiya Matsuzaka[2,4], Hajime Mushiake[2,3,4,5], Toru Ishizuka[1,2], Hiromu Yawo[1,2,3,5]***

**1** Department of Developmental Biology and Neuroscience, Tohoku University Graduate School of Life Sciences, Sendai, Japan, **2** Japan Science and Technology Agency (JST), Core Research of Evolutional Science & Technology (CREST), Tokyo, Japan, **3** Tohoku University Basic and Translational Research Center for Global Brain Science, Sendai, Japan, **4** Department of Physiology, Tohoku University Graduate School of Medicine, Sendai, Japan, **5** Center for Neuroscience, Tohoku University Graduate School of Medicine, Sendai, Japan

## Abstract

***Background:*** Optogenetic manipulation of a neuronal network enables one to reveal how high-order functions emerge in the central nervous system. One of the *Chlamydomonas* rhodopsins, channelrhodopsin-1 (ChR1), has several advantages over channelrhodopsin-2 (ChR2) in terms of the photocurrent kinetics. Improved temporal resolution would be expected by the optogenetics using the ChR1 variants with enhanced photocurrents.

***Methodology/Principal Findings:*** The photocurrent retardation of ChR1 was overcome by exchanging the sixth helix domain with its counterpart in ChR2 producing Channelrhodopsin-green receiver (ChRGR) with further reform of the molecule. When the ChRGR photocurrent was measured from the expressing HEK293 cells under whole-cell patch clamp, it was preferentially activated by green light and has fast kinetics with minimal desensitization. With its kinetic advantages the use of ChRGR would enable one to inject a current into a neuron by the time course as predicted by the intensity of the shedding light (opto-current clamp). The ChRGR was also expressed in the motor cortical neurons of a mouse using Sindbis pseudovirion vectors. When an oscillatory LED light signal was applied sweeping through frequencies, it robustly evoked action potentials synchronized to the oscillatory light at 5–10 Hz in layer 5 pyramidal cells in the cortical slice. The ChRGR-expressing neurons were also driven *in vivo* with monitoring local field potentials (LFPs) and the time-frequency energy distribution of the light-evoked response was investigated using wavelet analysis. The oscillatory light enhanced both the in-phase and out-phase responses of LFP at the preferential frequencies of 5–10 Hz. The spread of activity was evidenced by the fact that there were many c-Fos-immunoreactive neurons that were negative for ChRGR in a region of the motor cortex.

***Conclusions/Significance:*** The opto-current-clamp study suggests that the depolarization of a small number of neurons wakes up the motor cortical network over some critical point to the activated state.

**Citation:** Wen L, Wang H, Tanimoto S, Egawa R, Matsuzaka Y, et al. (2010) Opto-Current-Clamp Actuation of Cortical Neurons Using a Strategically Designed Channelrhodopsin. PLoS ONE 5(9): e12893. doi:10.1371/journal.pone.0012893

**Editor:** Vladimir Brezina, Mount Sinai School of Medicine, United States of America

**Received** June 4, 2010; **Accepted** August 31, 2010; **Published** September 23, 2010



**Funding:** Core Research for Evolutional Science and Technology (CREST), Japan Science and Technology Agency (JST): http://www.jst.go.jp/kisoken/crest/en/index.html. Grants-in-aid for scientific research from the Ministry of Education, Culture, Sports, Science and Technology (MEXT) of Japan, #21026002: http://www.nips.ac.jp/cellsensor/index.html. Global COE Program (Basic & Translational Research Centre for Global Brain Science), MEXT: http://sendaibrain.org/. Strategic Research Program for Brain Sciences (SRPBS), MEXT, #08030013: http://brainprogram.mext.go.jp/. The funders had no role in study design, data collection and analysis, decision to publish, or preparation of the manuscript.

**Competing Interests:** The authors have declared that no competing interests exist.

* E-mail: yawo-hiromu@m.tohoku.ac.jp

◔ These authors contributed equally to this work.

## Introduction

One of the enigmas in neuroscience is how high-order neural functions emerge from network communications among many neurons of various traits. To reveal this optical stimulating and recording methods are advantageous because of their high spatial and temporal resolutions [1,2]. Recently the optogenetics, which endows neurons with photosensitivity by genetic engineering methods, has opened new horizon in neural sciences [3–5].

Channelrhodopsin-1 (ChR1) and -2 (ChR2), which are involved in the light-dependent behavior of a unicellular green alga, *Chlamydomonas reinhardtii*, are unique in the family of archaeal-type rhodopsins [6–9], since each works as both photoreceptor and ion channel. Recently ChR2-mediated photostimulation of neurons has been applied to investigate the function of neural networks *in vivo* [10–13]. ChR2 can selectively activate neurons and is able to modify neuronal circuits by inducing synaptic plasticity. Moreover, ChR2-expressing transgenic animals have been generated and successfully used to study the neural basis of behavioral responses in *Caenorhabditis elegans* [14], zebrafish [15] and mammals [16,17]. Given its superiority in spatio-temporal resolution, ChR2 has become a powerful tool for the investigation of neural networks of various animals. ChR2 may also have potential as a visual prosthesis for photoreceptor degeneration [17]. In retinal degenerative diseases such as retinitis pigmentosa, photoreceptor cells are lost while the inner retinal neurons such as retinal ganglion cells and

bipolar cells are preserved. Exogenous expression of ChR2 in these neurons using viral vectors or *in vivo* electroporation methods restores visually-evoked responses in the visual cortex of rodents [18–20]. However, there are still some technological issues that need to be addressed to achieve the maximum potential of channelrhodopsins. First, photosensitive channels with various wavelength sensitivities would be desirable. Second, the prominent desensitization of ChR2 photocurrent limits its application for repetitive stimulation at high frequency. Third, the fast turning-on (ON) and -off (OFF) kinetics are ideal for manipulating membrane potential by light.

To manipulate optogenetically the neuronal activity, the ChR1 photocurrent has several advantages over the ChR2, such as the small desensitization and the rapid ON and OFF kinetics [8,9,21–23]. Unfortunately, it is small in amplitude because of the retarded membrane expression and other unresolved reasons [23,24]. Here we found that this retardation could be overcome by exchanging the sixth helix domain with its counterpart in ChR2 producing channelrhodopsin-green receiver (ChRGR) with further reform of the molecule. Since ChRGR showed smaller desensitization than ChR1 and the fast ON and OFF kinetics, it can be optimized for optogenetic injection of the patterned current into a neuron (opto-current clamp).

## Results

It has been suggested that the channel conductance or the probability of a channel being open is likely to be dependent on the sixth transmembrane helix of ChRs [23]. To test this, the sixth transmembrane domain ("*F*', Figure 1A) of ChR1 was replaced by its counterpart ("*f*') from ChR2 producing a chimera, ChR1-*f*. When expressed in HEK293 cells, this replacement enhanced the whole-cell conductance without changing the reversal potential and the action spectrum (Figure 1B–1C). In the middle of the seventh transmembrane helix of ChR1, $Lys^{296}$ is where the retinal is covalently binding. We subdivided the seventh transmembrane domain ("*G*') into two subdomains; one from $Leu^{270}$ to $Lys^{296}$ ("$G_1$") and the other from $Asn^{297}$ to $Glu^{345}$ ( "$G_2$"), then replaced each subdomain with its counterpart from ChR2 ("*g*'), $g_1$ ($Ile^{231}$-$Lys^{257}$) or $g_2$ ($Asn^{258}$-$Lys^{315}$). Each chimera channelrhodopsin, ChR1-$fg_1$ or ChR1-$fg_2$, was expressed in HEK293 cells and the action spectrum was again investigated. As shown in Figure 1E, the action spectrum of ChR1-$fg_2$ was almost identical to that of ChR1, whereas that of ChR1-$fg_1$ was blue-shifted (Figure 1F). The effective conductance of ChR1-$fg_2$ was 0.29±0.06 μS/pF (n = 10), as about 7-fold that of ChR1 (Figure 1C, 1D). Since the photocurrent size was variable from cell to cell, the averaged photocurrent was compared at 460 (0.027 $mWmm^{-2}$) and 520 nm (0.015 $mWmm^{-2}$). The photocurrent of ChR1-$fg_2$ was large at both wavelengths as expected from its effective conductance and the action spectrum (Figure 1G). In response to green light it generated relatively large photocurrents if compared to ChR2 or its gain-of-function variant ChR2-H134R [14], whereas in response to blue light their peak amplitudes were almost similar (Figure S1). Recently, one of channelrhodopsins derived from *Volvox* (VChR1) has been shown to have a red-shifted action spectrum [25]. Although its photocurrent is near maximal at 520 nm, the average photocurrent (−29±6 pA, n = 6) was smaller than that of ChR1-$fg_2$ (−146±38 pA, n = 8) with a significant difference (Figure S1).

Since the ChR1-$fg_2$, which we named channelrhodopsin-green receiver (ChRGR), generated photocurrents of relatively large amplitudes, it is a potential candidate of the optogenetic actuator by green light. To test this possibility, its photocurrent kinetics was investigated. Because the photocurrent kinetics are dependent on the light power density, the holding potential as well as the temperature, each photocurrent was measured at the holding potential of −40 mV and at 34°C, with various levels of light power density of green LED (505±15 nm, 1 s pulse, 0.064–0.77 $mWmm^{-2}$) (Figure 2A). The kinetic profile of ChRGR photocurrent was characterized by the ON kinetics, the desensitization and the OFF kinetics under comparison to those of ChR1 or 2 (Figure 2B, 2C). Quantitatively, the photocurrent ON kinetics, which followed a single exponential function, was evaluated by its apparent time constant ($\tau_{ON}$) as a function of the light power density (Figure 2D). The difference between the peak photocurrent and the steady-state photocurrent at the end of 1 s pulse was divided by the peak photocurrent amplitude, and the desensitization was evaluated as a function of the light power density (Figure 2E). Since the photocurrent OFF kinetics was best fitted by two exponential functions [23], it was evaluated by the effective OFF time constant ($\tau_{OFF}$), which is the time to reach $e^{-1}$ (37%) of the steady-state amplitude (Figure 2F). The photocurrents of ChRGR were rather similar to those of ChR1 than to those of ChR2 in their kinetic profiles. The recovery from the desensitization was examined by applying two 1 s light pulse (0.77 $mWmm^{-2}$) with variable intervals (Figure 2G). Both the peak and steady-state current was only little influenced by the preceding light exposure (Figure 2H and 2I) and the relatively rapid recovery of desensitized component with a time constant of 1.3 s (Figure 2J).

To manipulate optogenetically the neuronal activity the ChRGR has several advantages such as; (i) the small desensitization, (ii) the rapid recovery from desensitization, (iii) the rapid ON and OFF kinetics and (iv) the relatively large photocurrent evoked by light of long wavelength. These properties enable one to inject a current into a neuron by the time course as predicted by the intensity of the shedding light. That is, when the light is given in a square-pulse, a square-pulse current can be expected to be induced. When the light is given in a sinusoidal wave, a sinusoidal current can be expected to be induced. These optically induced currents would generate the membrane potential responses that are dependent on the neuron's membrane properties such as the membrane resistance, the membrane capacitance and the types of ion channels (opto-current-clamp). The membrane potential response is also dependent on the neuron's morphology, the distribution of intrinsic ion channels and the effective localization of ChRGR. We tested the opto-current-clamp using a ChRGR-expressing layer 5 (L5) pyramidal neuron of the mouse motor cortex. Neurons expressing ChRGR-Venus were found in layer II–VI of the cortex in 12 hours after injecting Sindbis pseudovirion vectors, were normal in appearance and their soma, dendrites and axons were fluorescently labeled (Figure 3A). One of the ChRGR-Venus-expressing L5 pyramidal neurons was identified in an acute slice of the cerebral cortex by its location, shape and size (Figure 3B). The fine processes such as axon, apical and basal dendrites, which were identified by the intracellular administration of biocytin (Figure $3C_i$), co-expressed ChRGR-Venus (Figures $3C_{ii}$ and $3C_{iii}$). Fine tufted dendrites with spines were also identified in layer I (Figure $3D_i$). These dendrites were also distinctly co-expressing ChRGR-Venus (Figure $3D_{ii}$ and $3D_{iii}$). However, its expression was indistinct in the spine. The membrane properties of the ChRGR-expressing neurons were the same as the non-expressing ones (Table S1) and direct current injection through the patch electrode evoked repetitive neuronal firings with almost the same frequency-current relationship (Figure S2A and S2B).

When a green LED pulse of 1-s duration was applied on the whole visual field, it evoked an inward current with minimal

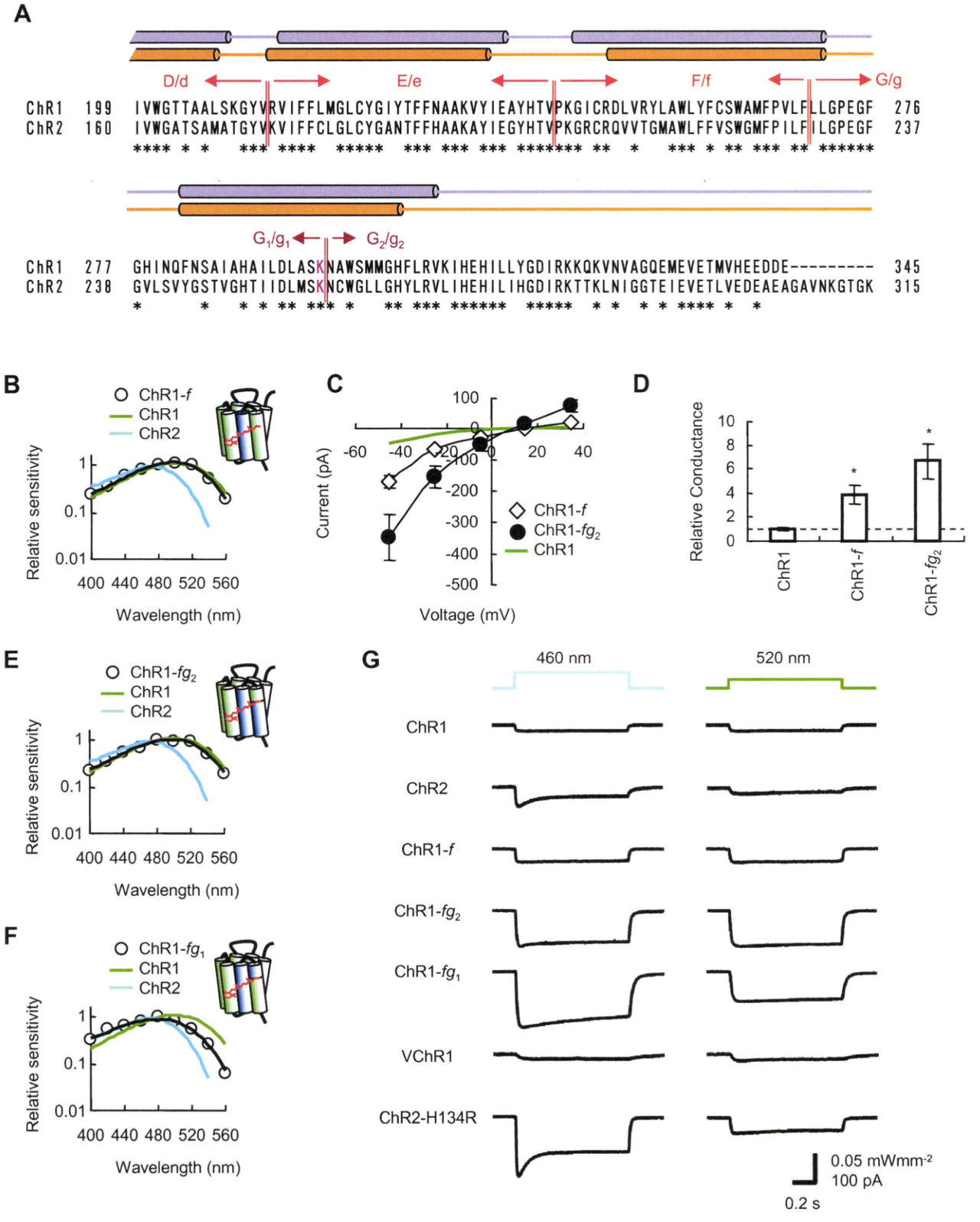


**Figure 1. Strategic design of channelrhodopsin-green receiver. A**. Sequence alignment of ChR1(199–345) and ChR2 (160–315). The identical amino acids are indicated with an asterisk (*). The putative fifth to seventh transmembrane domains, E/e to G/g, and subdomains are indicated. The putative transmembrane helixes are indicated by purple cylinders [24,25] or orange cylinders [7]. **B**. Action spectrum of ChR1-*f* photocurrent in comparison with ChR1 and 2. **C**. Photocurrent-voltage relationship. **D**. Summary of conductance relative to ChR1. Asterisks indicate statistical significance ($P<0.005$, Mann-Whitney *U*-test). **E** and **F**. Action spectrum of ChR1-$fg_2$ (E) and ChR1-$fg_1$ (F) photocurrents. **G**. Each trace is an average photocurrent evoked at either 460 or 520 nm. The number of samples are, 8 (ChR1), 8 (ChR2), 8 (ChR1-*f*), 8 (ChR1-$fg_2$), 8 (ChR1-$fg_1$), 6 (VChR1) or 9 (ChR2-H134R).

doi:10.1371/journal.pone.0012893.g001